# Thallium mass fraction and stable isotope ratios of sixteen geological reference materials

Alex **Brett** (1)*, Julie **Prytulak** (1), Samantha J. **Hammond** (2), Mark **Rehkämper** (1)
(1) Department of Earth Science and Engineering, Imperial College London, UK
(2) School of Environment, Earth and Ecosystem Sciences, The Open University, UK
* Corresponding author e-mail: a.brett13@imperial.ac.uk

***Abstract.*** Thallium stable isotope ratio and mass fraction measurements were performed on sixteen geological reference materials spanning three orders of magnitude in thallium mass fraction, including both whole-rock and partially-separated mineral powders. For stable isotope ratio measurements, a minimum of three independent digestions of each reference material were obtained. High-precision trace element measurements (including Tl) were also performed for the majority of these RMs. The range of Tl mass fractions represented is 10 ng $g^{-1}$ to 16 µg $g^{-1}$, and Tl stable isotope ratios (reported for historical reasons as $\varepsilon^{205}$Tl relative to NIST SRM 997) span the range -4 to +2. With the exception – attributed to between-bottle heterogeneity – of G-2, the majority of data are in good agreement with published or certified values, where available. The precision of mean of independent measurement results between independent dissolutions suggests that, for the majority of materials analysed, a minimum digested mass of 100 mg is recommended to mitigate the impact of small-scale powder heterogeneity. Of the sixteen materials analysed, we therefore recommend for use as Tl reference materials the USGS materials BCR-2, COQ-1, GSP-2, and STM-1; CRPG materials AL-I, AN-G, FK-N, ISH-G, MDO-G, Mica-Fe, Mica-Mg, and UB-N; NIST SRM 607; and OREAS14P.

***Keywords: thallium, stable isotopes, reference materials, powder heterogeneity, sample mass***

# INTRODUCTION

First isolated in 1861 (Crookes 1862, Lamy 1862), thallium is one of the highest atomic mass naturally-occurring elements: a volatile, highly incompatible trace metal, with two oxidation states available in addition to the neutral charge state. Univalent thallium ($Tl^{+}$) has a large ionic radius (1.49 Å), comparable to that of the alkali metals potassium, rubidium and caesium, and can therefore substitute for these elements in mineral crystal structures (Shaw 1952, Shannon and Prewitt 1969, Shannon 1976). Trivalent thallium ($Tl^{3+}$) can also exist on Earth under highly oxidising conditions (Bately and Florence 1975, Vink 1993), e.g. in the structure of the ferromanganese (Fe-Mn) mineral hexagonal birnessite (Peacock and Moon 2012, Nielsen *et al.* 2013).

Thallium has two stable isotopes with mass numbers 203 (29.5%) and 205 (70.5%). The relative difference in mass between thallium's two stable isotopes is less than 1%. Because the magnitude of mass-dependent stable isotope fractionations via kinetic and equilibrium processes scales inversely with both overall and relative mass difference (Bigeleisen and Mayer 1947, Urey 1947), it was assumed that there would be little mass-dependent thallium isotope fractionation in nature. Resolvable Tl isotopic differences were therefore thought to arise solely due to decay of the relatively short-lived radioisotope $^{205}Pb$ to $^{205}Tl$, with a half-life of about 15 Ma. Initial investigations (Anders and Stevens 1960, Chen and Wasserburg 1987,1994, Huey and Kohman 1972, Ostic *et al.* 1969) thus aimed to provide constraints on the delivery and distribution of $^{205}Pb$ during the early stages of solar system formation by tracking differences in Tl isotope ratios. These efforts proved unable to resolve variations for a large number of extraterrestrial and some selected terrestrial materials. This inability was for the most part due to the uncertainties (>2‰, 2*s*) associated with TIMS measurement results of Tl (see summary in Nielsen *et al.* 2017).

As a consequence of initial development of the system in the context of cosmochemistry, where

small radiogenic isotope variations are routinely reported using $\varepsilon$-notation, Tl isotope ratios are traditionally reported relative to the NIST Tl reference material SRM 997 (defined as 0) as

$$\varepsilon^{205}Tl_{SRM997} = 10{,}000 \times [(^{205}Tl/^{203}Tl_{sample} - {}^{205}Tl/^{203}Tl_{SRM997})/(^{205}Tl/^{203}Tl_{SRM997})]$$

Strictly, use of $\varepsilon$-notation is deprecated in favour of $\delta$-notation (Coplen 2011), whereby

$$\delta^{205}Tl_{SRM997} = \delta^{205/203}Tl_{SRM997} = [R(^{205}Tl/^{203}Tl_{sample}) - R(^{205}Tl/^{203}Tl_{SRM997})]/R(^{205}Tl/^{203}Tl_{SRM997})$$

However, since 1999 all published Tl isotope data has been reported using $\varepsilon^{205}Tl_{SRM997}$, which is strictly equivalent to $\delta^{205}Tl_{SRM997}$ in parts per ten thousand. The universal convention of reporting $\varepsilon^{205}Tl_{SRM997}$ is therefore maintained here for ease of comparison with Tl isotope ratio literature.

The development of multi-collector ICP-MS (MC-ICP-MS) allowed for higher-precision Tl isotope ratio measurements, with precisions >3-4 times better than those achieved by the best TIMS protocols then reported (0.1-0.2 ‰, 2*s;* Arden 1983). Using these new measurement principles, Rehkämper and Halliday (1999) analysed a number of terrestrial samples in order to define the baseline terrestrial Tl isotope composition for the purpose of comparison with extraterrestrial materials, again assuming that variations in extraterrestrial materials would reflect early $^{205}$Pb decay. They unexpectedly discovered large variations in Tl isotope ratios for terrestrial materials, from $\varepsilon^{205}Tl_{SRM997}$ -1.8 ± 1.9 (2*s*) to 11.9 ± 0.5 (2*s*).

The natural range of Tl stable isotope variations documented on Earth now exceeds 35 $\varepsilon^{205}Tl_{SRM997}$ units ("$\varepsilon$-units"; see review in Nielsen *et al.* 2017). With the exception of volcanic fumaroles and some meteorites (Baker *et al.* 2009,2010b, Nielsen *et al.* 2006a), these variations are best explained by equilibrium isotope effects (Nielsen *et al.* 2006c, Rehkämper *et al.* 2002). The magnitude of equilibrium stable isotope variation in Tl exceeds those predicted by classical models of mass-dependent isotope fractionation. Schauble (2007) showed that, for very heavy elements including thallium, variation in nuclear volume means that neutron-rich isotopes tend to be concentrated in more oxidised species. A combination of mass-dependent and nuclear volume effects therefore accounts for the stable isotope fractionation displayed by Tl (e.g. Fujii *et al.* 2013). Stable isotope variations arising due to this “nuclear field shift effect” (King 1984) have also been documented for

other very heavy elements, including Hg (Smith *et al.* 2005, Xie *et al.* 2005, Moynier *et al.* 2013) and U (Fujii *et al.* 1989a,b, Stirling *et al.* 2007, Moynier *et al.* 2013). Additionally, recent calculations (Yang and Liu 2015) suggest that the nuclear volume effects may produce large differences (up to approximately 4‰) for Pb in systems containing $Pb^{4+}$- and $Pb^{2+}$-bearing species.

As of 2018, there are more than 30 studies utilising Tl isotope ratio variations to investigate the natural environment. The utility and versatility of the system lies in the large isotope ratio differences and relatively high mass fractions (μg $g^{-1}$) associated with low temperature environments, in contrast with very low mass fractions and negligible isotope ratio differences in mantle-derived lavas (see review of Nielsen *et al.* 2017, Prytulak *et al.* 2017). Applications include investigations of extraterrestrial materials (Andreasen *et al.* 2009, 2012, Baker *et al.* 2010b, Nielsen *et al.* 2006a, Palk *et al.* 2011); riverine and marine fluxes (Nielsen *et al.* 2004, 2005, 2006c, Owens *et al.* 2016, Rehkämper *et al.* 2002, Rehkämper and Nielsen 2004); anthropogenic mobilization of Tl (Kersten *et al.* 2014, Nriagu 1998, Peter and Viraraghavan 2005, Vaněk *et al.* 2018, Xiao *et al.* 2003, 2004); ore exploration (Baker *et al.* 2010a, Hettmann *et al.* 2014); and use as a tracer of contributions to the source regions of igneous materials (Nielsen *et al.* 2006b, 2014, 2015, 2016, Prytulak *et al.* 2013, 2017, Shu *et al.* 2017, Blusztajn *et al.* 2018).

Despite the breadth of study, literature reports of thallium isotope ratios for geological reference materials have been restricted to three basalts, one andesite and one granite (Table 1), in addition to two ferromanganese sediments, one meteorite and one seawater sample. In response to the growing application of thallium isotopes in Earth systems, we provide the first measurement results of Tl isotope ratios for the bulk rock reference materials COQ-1, GSP-2, ISH-G, MDO-G, STM-1, and UB-N alongside determinations for previously analysed bulk rock reference materials BCR-2, BHVO-2, and G-2. Investigations of emerging stable isotope systems commonly reveal equilibrium inter-mineral isotope fractionations at high temperatures, as reviewed in Teng *et al.* (2017). We therefore also present the first determinations of Tl mass fractions and isotope ratios for the mineral reference materials 14P, AL-I, AN-G, FK-N, NIST SRM 607, Mica-Fe, and Mica-Mg, in an effort

to establish an estimate of the possible magnitude of stable isotope ratio variation in phases potentially rich in Tl. These reference materials are intended to be used as matrix-matching RMs for future investigations rather than be interpreted in isolation as indicative of natural Earth processes. A minimum of three separate digestions, separations and measurements were performed for each RM. With the exception of 14P, the reference materials were also analysed for high precision trace element mass fractions, including thallium. We focus on reference materials useful for high temperature applications. Table 2 provides background information on each selected material.

## EXPERIMENTAL PROCEDURE

### *Determination of Tl isotope ratios*

**Reagents:** All sample digestions and chemical separations were carried out in the MAGIC Laboratories, Imperial College London. Purified water from a Milli-Q® (Merck) system (resistivity 18.2 MΩ cm) was used throughout. $HNO_3$ (concentrated, ~14 mol $l^{-1}$) and HCl (6 mol $l^{-1}$) were purified once by sub-boiling distillation in quartz or PTFE stills, whilst ultrapure HF (47–51% ≈ 24 mol $l^{-1}$) was either purchased from SCP Scientific or prepared in the laboratory from reagent-grade acid by a single distillation step in a PTFE still. Saturated bromine water was prepared by the equilibration of high-purity bromine with purified water in a 125 ml PTFE bottle. Dilute $HNO_3$ and HCl containing 1–3% v/v saturated bromine water were prepared by adding the appropriate volume of bromine water to the acid immediately before use. A solution of 5–6 % w/w $SO_2$ in 0.1 mol $l^{-1}$ HCl ("0.1 mol $l^{-1}$ HCl–5% $SO_2$") was used for the reductive elution of Tl from anion-exchange resin. This solution was prepared in a 250 ml PTFE bottle containing 100-200 ml 0.1 mol $l^{-1}$ HCl, through which was bubbled gaseous $SO_2$ from a small pressurised cylinder containing liquefied $SO_2$ (purchased from Sigma Aldrich). The solution was reweighed at regular intervals until the required amount of $SO_2$ had dissolved in the acid. After preparation, the reagent was stored for a maximum of 1 week for reuse then discarded, as $SO_2$ oxidises to form sulphate. Finally, a 0.1 mol $l^{-1}$ $HNO_3$–

0.1% v/v $H_2SO_4$ solution used for sample dilution and subsequent mass spectrometric measurement was made up using distilled-grade concentrated $H_2SO_4$ (96 % v/v).

**Sample digestion:** Between 25 mg and 350 mg of reference material powder was accurately weighed into PFA vials (Savillex®), depending on the mass fraction of Tl in the RM. The majority of digestions (exceptions detailed below) were performed on a tabletop hotplate (quoted temperatures are the hotplate temperature setting, unless otherwise specified) at 140 °C for 1-3 days, in an initial mixture of 3 ml HF (24 mol $l^{-1}$) and ~0.3–0.5 ml $HNO_3$ (14 mol $l^{-1}$). Samples were then evaporated to near (rather than total) dryness, to minimise formation of insoluble fluorides (Croudace 1980, Yokoyama *et al.* 1999); taken up in ~1 ml of $HNO_3$ (14 mol $l^{-1}$); and evaporated to dryness at 180 °C at least three times, to destroy any fluorides formed and to evaporate $SiF_4$. Samples were redissolved and evaporated once from 4 ml HCl (6 mol $l^{-1}$) at 120 °C; redissolved in 2 ml HCl (6 mol $l^{-1}$) and refluxed at 120 °C for a minimum of 12 hours; and finally made up to a 12 ml HCl (1 mol $l^{-1}$) solution subsequently used to load into the first separation column. The final loading solution of 12 ml HCl (1 mol $l^{-1}$) for column chromatography was refluxed at 140 °C for a minimum of 12 hours. Sample solutions were cooled and 400 µl of saturated $Br_2$ water was added, then left for a minimum of 3 hours to ensure complete oxidation of thallium to its $Tl^{3+}$ state.

Some of the investigated RMs (COQ-1, G-2, GSP-2, ISH-G, MDO-G, STM-1) contain refractory phases such as zircon that may not be completely digested using hotplate dissolution alone. Although thallium is not expected to reside in phases such as zircon, we investigated the potential role of refractory phases on Tl mass fraction and isotope ratio by performing bomb digestions. To this end, approximately 50 mg of powder was accurately weighed into PFA hexagonal bomb vials (Savillex®), to which was added ~0.2 ml $HNO_3$ (14 mol $l^{-1}$) and 1.5 ml HF (24 mol $l^{-1}$). The prepared bombs were sealed tightly and placed in an oven at 150 °C for five days. Subsequent sample processing was identical to that for hotplate digestions.

The massive magmatic sulphide 14P was digested on a hot plate at 130°C for a minimum of 12 hours in ~5 ml $HNO_3$ (3 mol $l^{-1}$), after the protocol of Nielsen *et al.* (2011). Samples of 14P were then evaporated to near dryness at 155 °C and redissolved in 12 ml HCl (1 mol $l^{-1}$). The solution was then centrifuged and detrital residue was discarded.

**Chromatographic separation of Tl:** Separation of the Tl fraction from sample matrices largely follows the two-stage ion-exchange procedure devised by Rehkämper and Halliday (1999) and refined by Nielsen *et al.* (2004) (Table 3). The separation technique utilizes the two oxidation states of thallium. Oxidised $Tl^{3+}$ adsorbs much more strongly to anion resins than $Tl^{+}$ under a variety of conditions, with a general decrease in distribution coefficients with increasing HCl concentration (Kraus *et al.* 1954). Experimental work by Horne (1958) established that at a temperature of 25 °C the distribution coefficient of $Tl^{3+}$ on Dowex® 1-X8 from aqueous HCl solutions ($10^{-3}$ to 2 mol $l^{-1}$) has values of $D \geq 10^5$. Under identical conditions the distribution coefficient for $Tl^{+}$ is much smaller; the maximum value ($D = 10^3$) occurs for 1 mol $l^{-1}$ HCl, and decreases rapidly with small variations in HCl concentration. Horne (1958) also observed that adsorption of $Tl^{3+}$ onto Dowex® 1-X8 from HBr media was too strong to be reliably measured. Thus the ion-exchange procedure employs HCl (at concentrations ≤2 mol $l^{-1}$) and $HNO_3$ admixed with 1-3% v/v saturated bromine water for sample loading and elution of major and trace elements, to ensure that all Tl remains strongly adsorbed to the resin as $Tl^{3+}$ complexed with chloride and trace bromide present in the bromine solution.

Collection of the thallium fraction is accomplished using a solution of 0.1 mol $l^{-1}$ HCl–5% $SO_2$ (see **Reagents**). This reduces $Tl^{3+}$ to $Tl^{+}$, whereby the latter can be readily eluted from the column. Yields of >95% are routinely achieved (Nielsen *et al.* 2004, Rehkämper and Nielsen 2004), with no isotopic fractionation of the separated Tl with respect to the original sample (Rehkämper *et al.* 2002, Nielsen *et al.* 2004).

Here the resin used is AG® 1-X8 (200–400 mesh) anion resin. The resin is cleaned prior to use in 4 mol $l^{-1}$ $HNO_3$ (3 times), 18 MΩ cm water (3 times), quartz-distilled 6 mol $l^{-1}$ HCl (once), and again in 18 MΩ cm water (3 times); finally, the resin is stored in quartz-distilled HCl (0.1 mol $l^{-1}$). Between each stage of cleaning the resin is left to stand for five days with intermittent shaking. A fresh resin bed is prepared for each separation and a two-stage process is used (i) to ensure complete elution of other ions and particularly of Pb, and (ii) to minimise the amount of sulphuric acid present prior to measurement.

Table 3 outlines the two-step chromatographic procedure. Briefly, the first stage of separation utilises quartz columns with an inner diameter 6 mm, fitted with quartz wool plugs for support of the resin bed, which is filled with 1000 µl resin (wet volume). Once collected in acid cleaned PFA vials, the Tl fraction is evaporated at 200 °C, which leaves <20 µl residual concentrated $H_2SO_4$, formed via oxidation of $SO_2$ used during collection of Tl. The sample is then re-dissolved in a few drops (~0.1 ml) of concentrated HCl (12 mol $l^{-1}$), and evaporated again at 200 °C to reduce the amount of residual $H_2SO_4$. Subsequently, the Tl fraction is dissolved in 1.5 ml HCl (1 mol $l^{-1}$) and refluxed for 12 hours at 140 °C. Once cooled, 60 µl of saturated $Br_2$ water is added to this solution; the sample is then left for a minimum of 3 hours to ensure complete oxidation of all Tl ions to the $Tl^{3+}$ state.

The second stage of chromatographic separation is a scaled-down version of the first column, to provide a final “clean-up” of matrix elements from the Tl fraction. Shrink-fit PFA columns fitted with polypropylene frits are filled with 150 µl resin. Once collected, the Tl fraction is evaporated to near dryness on a hotplate set at 200 °C, leaving <10 µl residual concentrated $H_2SO_4$. The residue is taken up in a few drops (~0.1-0.3 ml) $HNO_3$ (14 mol $l^{-1}$) and evaporated to dryness at 200 °C three times, in order to remove as much of the remaining sulphuric acid and chloride ions as possible.

**MC-ICP-MS isotope ratio measurements:** The use of PFA beakers and the high evaporation

temperature of $H_2SO_4$ means that it is not possible to remove all $H_2SO_4$ from the Tl fraction by evaporation. Nielsen *et al.* (2004) demonstrated that analytical artefacts of up to 1 ε-unit can be generated if $H_2SO_4$ is present in samples but not in bracketing standards. Therefore, all sample residues were dissolved in 1 ml of 0.1 mol $l^{-1}$ $HNO_3$-0.1% v/v concentrated $H_2SO_4$ for isotopic analysis. The mass bias-corrected $^{205}Tl/^{203}Tl$ ratio is essentially independent of the concentration of $H_2SO_4$ up to 1% v/v (Nielsen *et al*. 2004). Reference solutions were prepared using the same batch of 0.1 mol $l^{-1}$ $HNO_3$-0.1% v/v concentrated $H_2SO_4$ to minimise matrix mismatch between samples and reference solutions. Isotopic ratio measurements were carried out using a Nu Instruments (HR) MC-ICP-MS in low resolution mode at the MAGIC Laboratories, Imperial College London. Sample introduction systems used over the course of this study include the Aridus, Aridus II and Nu Instruments DSN (Desolvation Nebuliser System), coupled with either PTFE or glass nebulisers, with measured uptake rates between 70 and 120 µl $min^{-1}$. Samples are run in a sequence using a Cetac autosampler. Dedicated PFA autosampler vials are used for all reference and wash solutions. Sample solutions are made up in 3 ml acid-cleaned PP autosampler vials.

Thallium has only two stable isotopes, precluding the possibility of isotopic spiking. Sample-standard bracketing was therefore employed by interspersing unknown samples between analyses of NIST SRM 997 (defined as $\varepsilon^{205}Tl_{SRM997} = 0$) at the same mass fraction and with the same acid matrix (i.e., a “matching standard”).

The ion beams at m/z 202 ($Hg^+$), 203 ($Tl^+$), 204 ($Pb^+$ with possible $Hg^+$ interference), 205 ($Tl^+$), 206 ($Pb^+$), 207 ($Pb^+$) and 208 ($Pb^+$) were monitored simultaneously with the Faraday collectors L2, L1, Ax, H1, H2, H3 and H4, all fitted with $10^{11}$ Ω resistors. Data collection was performed in three blocks of 20 cycles with 5s integrations with the electrostatic energy analyser (ESA) deflected for a 15s electronic baseline at the beginning of each block.

An external means of monitoring and correcting for mass bias must be employed when measuring

an element with only two stable isotopes. In the case of thallium, samples and standards are doped with NIST SRM 981 Pb. The certified $^{208}Pb/^{206}Pb$ isotope amount ratio is used to carry out on-line correction for mass discrimination of the measured $^{205}Tl^{+}/^{203}Tl^{+}$ ratio during the measurement. The Pb/Tl mass fraction ratio of samples and standards was between 3 and 4, and matched to within 15%, as variations in the Pb/Tl mass fraction ratio may cause real or apparent changes in the mass bias response of Pb and Tl (Rehkämper and Mezger 2000). This methodology is analogous to the use of Tl doping when performing Pb isotope ratio measurements via MC-ICP-MS (e.g. Rehkämper and Mezger 2000, White *et al.* 2000). Typical instrument sensitivity was between 600 and 900V per $\mu g\ g^{-1}$ of Pb or Tl. The repeatability of bracketing SRM 997 reference solutions degrades significantly with $^{205}Tl^{+}$ beam intensities below 1V. Therefore, sample solutions were prepared with typical Tl mass fractions of 3-5 ng $g^{-1}$ and Pb mass fractions between 15-20 ng $g^{-1}$.

Machine performance is monitored by measurement of a Tl secondary standard solution obtained from Aldrich and first characterised by Rehkämper and Halliday (1999) ("Aldrich Tl solution"), which has subsequently been analysed repeatedly (>2000 times) in at least seven laboratories worldwide (see compilation of Nielsen *et al.* 2017). A minimum of three measurements of the Aldrich Tl solution were performed at the beginning and end of each measurement session, and periodically throughout - typically every four to six unknown sample measurements. A well-characterised USGS RM (typically BCR-2) was processed through the complete sample preparation procedure with every batch of samples prepared for MC-ICP-MS analysis. Thallium mass fractions and $\varepsilon^{205}Tl_{SRM997}$ values were compared against in-house and inter-laboratory long-term averages, to assess trueness and long-term precision.

**MC-ICP-MS Tl mass fraction estimates**: Estimates of thallium mass fractions were acquired during MC-ICP-MS measurements of Tl isotope ratios by comparison of ion beam intensities between reference solutions of known mass fraction and unknown samples, assuming chemical separation returns 100% thallium yields. In detail, the Tl mass fractions were estimated based on measurements of Pb/Tl mass fraction ratios using the known absolute mass of NIST SRM 981 Pb

added to sample and reference solutions. However, these measurements are sensitive to small variations in sample dilution, which may occur during sample preparation due to (i) small variations between pipette tips and pipettes; (ii) differences in the volume consumed during initial concentration checks of the diluted sample (for standard-matching purposes); (iii) variations how long a sample is left to stand in the autosampler before a measurement is made (i.e. how much evaporation occurs prior to measurement).

Materials such as the sulphide 14P cannot reasonably be analysed for trace elements on quadrupole or sector field ICP-MS instruments dedicated to silicate analyses due to memory effects associated with very high iron and sulphur mass fractions. It is also difficult to calibrate and matrix-match this type of material. This is not, however, a concern when measuring a purified Tl fraction via MC-ICP-MS. Thus, the Tl mass fraction of 14P is reported based on the estimations made during MC-ICP-MS isotopic ratio measurement, with correspondingly higher uncertainty. Overall, the trueness of such Tl mass fraction estimates have been improved from ~25% (Rehkämper *et al.* 2002, Rehkämper and Nielsen 2004) to ~5-10% (e.g. Prytulak *et al.* 2013, Shu *et al*. 2017) provided care is taken during sample handling. However, ICP-MS analysis with well-characterised calibrating standards and/or standard addition techniques returns the least biased and most precise Tl mass fraction data.

*Determination of Tl mass fraction by ICP-MS/MS ('ICP-QQQ-MS' or 'triple quad')*

Reference material digestions were undertaken in the MAGIC Laboratories at Imperial College London, using the same reagents employed for isotope analyses.

**Method:** Approximately 50 mg of each RM was weighed accurately into PFA vials, to which a 3:1 mixture of HF (24 mol $l^{-1}$):$HNO_3$ (14 mol $l^{-1}$) was added. The solutions were ultrasonicated for 20 minutes after initial addition of the acids, then placed on a hotplate at 160 °C for at least 24 hours. Sample solutions were further ultrasonicated for 20 minutes twice during the initial digestion.

Solutions were then evaporated to near dryness, redissolved in 2 ml of HCl (6 mol $l^{-1}$), and refluxed at 120 °C for at least 24 hours. The solutions were next evaporated to complete dryness at 120 °C, redissolved in 1 ml of $HNO_3$ (14 mol $l^{-1}$), and then evaporated at 180 °C. The last step was repeated a minimum of three times, or until the colour of the residue changed from white to brown, which indicates that fluorides formed from the initial HF digestion have been destroyed. Samples were then transported to the Open University as $HNO_3$ (14 mol $l^{-1}$) solutions, and transferred into acid-cleaned PP bottles, where an appropriate amount of purified $H_2O$ was added to each to achieve a 1000-fold dilution of the original sample mass in an $HNO_3$ matrix (0.14 mol $l^{-1}$).

**ICP-QQQ-MS measurement:** Trace element mass fraction determinations including thallium were undertaken at the Open University, UK, with an Agilent 8800 ICP-QQQ-MS inductively-coupled plasma mass spectrometer. Sample solutions were aspirated using a quartz microflow nebuliser with an uptake rate of 0.5ml $min^{-1}$. Machine sensitivity was on the order of 1 – 5 x $10^7$ cps per µg $ml^{-1}$, depending on the element. The Agilent 8800 has a collision/reaction cell (Octopole Reaction System, ORS), which separates two quadrupoles. The first quadrupole is used as a mass filter to ensure that only specific masses enter the ORS; reactions can therefore be targeted to remove on-mass interferences. The second quadrupole can be used in either mass-shift or on-mass mode, depending on if the analyte or interference reacts with the gas. We employ two collision/reaction gas configurations to undertake measurements: no gas in the collision cell or $O_2$ gas in the cell. Thallium was analysed in the 'no gas' mode, with oxide levels (measured as $CeO^+/Ce^+$) kept below 1% and double charged species ($Ce^{2+}/Ce^+$) at 1.6%. All other elements were similarly measured except for most rare earth elements (La, Pr, Ce, Nd, Sm, Gd, Ho, Tb, Dy, Er, Yb, Lu), which were reacted with $O_2$ gas for a mass shift measurement.

**Selection and assessment of calibrating standards:** Calibrating standards were run at the beginning of each measurement session. Additionally, an internal solution standard consisting of Be, Rh, In, Tm, Re, and Bi was added online to all standard and unknown solutions to monitor and correct instrumental drift. Drift was further monitored every five unknown measurements with a

measurement block consisting of BIR-1 (a separate digestion to that used in the initial calibration block), $HNO_3$ (0.3 mol $l^{-1}$), and a repeated unknown sample.

The USGS reference materials BIR-1, BHVO-2 and AGV-1 were chosen as calibrators for trace element determination of Tl in particular. In addition, RMs W-2 and DNC-1 are used for calibration: for most trace elements (not including Tl) these are well-characterised materials. BIR-1, BHVO-2 and AGV-1 were selected because they are commonly used for analysis of other isotopic systems, i.e. they are well-characterised, and span three orders of magnitude of Tl mass fraction. Only AGV-1 has a USGS listed Tl mass fraction (0.34 µg $g^{-1}$, recommended value; no uncertainty given). All three RMs have preferred GeoReM (Jochum *et al.* 2005) Tl mass fraction values, per Jochum *et al.* (2016): BIR-1, 2.1 ± 0.7 ng $g^{-1}$ (n = 13); BHVO-2, 22.4 ± 1.5 ng $g^{-1}$ (n = 28); AGV-1, 337 ± 31 ng $g^{-1}$ (n = 10) (95% confidence intervals). Specifically, we use Tl mass fractions of: BIR-1, 1.6 ng $g^{-1}$ (n = 12); BHVO-2, 22 ng $g^{-1}$ (n = 32); and AGV-1, 349 ng $g^{-1}$ (n = 13), determined using our own compilation of reported mass fraction data (Appendix 1). All values are within error of the GeoReM recommended values.

We note that both AGV-1 and BHVO-2 exhibit heterogeneity seen in Pb isotope ratio and mass fraction results, which have been provisionally attributed to contamination during processing using steel mortar and pestle (Weis *et al.* 2006). It has long been suggested that the similarity between properties of Tl and Pb might result in similar behaviours in some geochemical contexts (Lamy 1862), but as Tl has historically not been routinely analysed it is not clear whether Tl systematics in these RMs correlate with Pb heterogeneity. We therefore use our compilation of reported Tl mass fractions in these RMs (Appendix 1) to identify and characterise potential Tl heterogeneity in our calibrators.

We find no identifiable heterogeneity for AGV-1 (n = 13, RSD = 15%). Reported BIR-1 Tl mass fraction results have a notably high RSD (34%); however, this material has a very low Tl mass

fraction and is therefore analytically challenging. Consequently, determining whether the high uncertainty reflects powder inhomogeneity or analytical error is not straightforward, and BIR-1 remains the best-characterised candidate for a low mass fraction Tl calibrator. For BHVO-2 there is some variation in reported Tl mass fraction between studies: of the 36 reported measurement results (mean mass fraction value of 28 ng $g^{-1}$; RSD = 58%), a small minority (n = 4) have a mean of 65 ng $g^{-1}$ (RSD = 7%). The remaining measurement results give a mean of 22 ng $g^{-1}$ (RSD = 20%). For comparison, BHVO-1 has a reported Tl mass fraction of 46 ng $g^{-1}$ (RSD = 19%, n = 25). The four anomalous reports of Tl mass fraction in BHVO-2 (Bouman *et al.* 2004, Deegan *et al.* 2012, Deng *et al.* 2013 and Søager *et al.* 2015) are suggestive of either confusion between the two generations of the BHVO RM, or of possible contamination.

For many trace elements, BHVO-1 and BHVO-2 have USGS listed mass fraction values that are within error of one another. Elements for which this is not true, where analysed, can be used to positively identify instances of confusion between the two generations. For the majority of these elements (notably Sc, Cr, Cu, Zn, Y, Zr and Hf as well as Tl) the mass fractions reported by Bouman *et al.* (2004) as BHVO-2 are highly consistent with listed values for BHVO-1, and disagree with listed values for BHVO-2; the reported Tl mass fraction is 59 ng $g^{-1}$. Only USGS listed BHVO-2 values are quoted as reference mass fractions for trace element analyses, and these do not include a Tl mass fraction; however, the same paper employs BHVO-1 as a Li isotope RM, suggesting a source of possible confusion. Similar is true for the trace element mass fractions reported by Deng *et al.* (2013), and in this case it appears that the quoted reference Tl mass fraction is *not* for BHVO-2, but instead that given for BHVO-1 by Govarindju (1994). Deng *et al.* (2013) report a Tl mass fraction of 66 ng $g^{-1}$ for BHVO-2.

For the two remaining anomalous reports of Tl mass fraction, the trace element pattern is less suggestive of confusion between generations of this reference material. Trace element mass fractions reported by Deegan *et al.* (2012) are on average 10% higher than USGS listed values (2%-20% higher), with the exception of Ta, which is in agreement with the listed value. Two Tl mass

fractions are reported for BHVO-2, of 60 ng $g^{-1}$ and 80 ng $g^{-1}$. Søager *et al.* (2015) used reference values provided by the Hamburg laboratory that performed sample analysis (pers. comm., 2017), and report a Tl mass fraction for BHVO-2 of 63 ng $g^{-1}$. These Tl mass fractions are anomalously high for BHVO-2, but are consistent with the listed and compiled values for BHVO-1; however, there is no compelling indication that in these cases confusion between the two generations of powder occurred. These results therefore appear to be best explained by some combination of analytical uncertainty and powder contamination.

The available data therefore suggest that if BHVO-2 suffers from inhomogeneity with respect to Tl mass fractions, it is not a widespread or common problem. Furthermore, there are very few generally-available igneous standard RMs with low Tl mass fractions. BIR-1, with a Tl mass fraction an order of magnitude lower than BHVO-2, is employed as a calibrator in this study, but as noted presents analytical challenges. The Geological Society of Japan provides three basalt RMs, but all have higher Tl mass fractions than BHVO-2: JB-2 has the lowest Tl mass fraction, reported as 34 ± 3.6 ng $g^{-1}$ (Jochum *et al.* 2016). As such, BHVO-2 is the best widely-available, well-characterised choice for a low-Tl calibrating standard.

Trace element mass fractions were generally determined with the chosen geological calibrating standards (AGV-1, BHVO-2, BIR-1). However, partially-separated mineral standards have unusual and, in some cases, extreme trace element mass fractions. For example, a Tl mass fraction of 16 µg $g^{-1}$ was reported for the biotite Mica-Fe (Table 4), well outside the Tl mass fraction range of the calibrators. Linear extrapolation of the calibration curve is a potential source of error for the reported mass fractions of such high-Tl RMs. Two approaches that are potentially suited to address this concern are (i) isotope dilution ICP-MS (ID-ICP-MS), and (ii) the use of synthetic calibrating reference solutions with known, high Tl mass fractions. The ID-ICP-MS technique was not deemed appropriate, due to the lengthy preparation times required and the possible powder heterogeneity of at least some samples. In other words, obtaining highly accurate trace element mass fraction data for a single dissolution of a potentially heterogeneous material is deemed to be of limited utility. In

contrast, the use of synthetic calibrating standards requires significantly less preparation time. However, it is known that the sample matrix can affect the ionisation potential of elements during analysis and, consequently, mass fraction measurement results (e.g. Brown and Milton 2005). To the best of our knowledge it has not previously been established whether using synthetic calibrators results in any systematic effect on measured Tl mass fractions. Therefore, for one analytical session a pure internal trace element reference solution (made from single element plasma grade standards (Alfa Aesar)) was employed as a synthetic calibrating reference solution to assess whether this procedure produced Tl mass fraction data that differed significantly from those obtained with geological calibrators.

# RESULTS AND DISCUSSION

*Determination of Tl mass fraction*

**Mass fraction measurements by ICP-QQQ-MS:** Table 4 presents the thallium mass fractions determined for RMs in this study, whilst Appendix 2 gives trace element results. Typical precisions reported for Tl in the literature are on the order of 5-15% RSD, compared with <5% RSD for commonly-analysed trace elements. Precision is normally deemed excellent if RSDs are <3% or good if 3-7%.

RSDs for Tl mass fraction measurement results obtained during this study using ICP-QQQ-MS with geological calibrating standards are calculated as follows. (i) Where the number of measurements $n > 4$, the RSD is calculated using the mean and standard deviation of those $n$ analyses. (ii) Where $n = 1$, the reported RSD is based on the within-run standard deviation of the five ICP-QQQ-MS mass scans that comprise each individual analysis. (iii) For $1 < n < 5$, RSDs calculated using method (i) are compared with the within-run standard deviation for each of the $n$ analyses, and the worse of the

two precisions is reported.

With the exception of three RMs (AL-I, AN-G and BIR-1), RSDs for Tl mass fraction measurement results obtained during this study using ICP-QQQ-MS with geological calibrating standards are <7%, and all RSDs except that for BIR-1 are <10% (Appendix 2). We note that RM AN-G has a low Tl mass fraction (10 ng $g^{-1}$, RSD = 8.1%), making precise measurements technically challenging. Similarly, BIR-1 has a very low Tl mass fraction (1 ng $g^{-1}$); even for this material, an RSD (n = 18) of 21% is achieved. Multiple dissolutions were analysed for trace element mass fractions using ICP-QQQ-MS for BCR-2 (multiple hotplate digestions), BHVO-2 (multiple hotplate digestions measured as unknowns, in addition to the calibrator solution), and GSP-2 (hotplate and bomb digestions). Notably, the hotplate versus bomb dissolution of GSP-2 showed no resolvable variation of Tl mass fraction with digestion method (RSD = 4.5%), suggesting, as expected, that Tl is not hosted in refractory phases present in this material (Appendix 2).

Analyses employing synthetic calibration reference solutions produced measured Tl mass fractions that are 10 ± 3% (1*s*) lower than the exact same sample solutions measured relative to geological reference materials (Figure 1) for all samples except AN-G. This suggests that the presence of a geological matrix alters the ionisation potential of Tl relative to synthetic trace-element reference solutions. Indeed, the 10 ± 3% (1*s*) offset in mass fractions observed is apparent even for those materials that fall within the Tl mass fraction range of the geological calibrators employed. Therefore, despite the fact that using geological RMs is a more time-consuming process and that linear extrapolation must be employed with caution, we recommend using geological rather than synthetic calibrators to avoid under-reporting of Tl mass fractions.

**Mass fraction measurements by MC-ICP-MS**: Mass fraction measurements made during isotope ratio analysis via MC-ICP-MS are iindistinguishable from ICP-QQQ-MS results, but show substantial variance (Figure 2) with RSDs (calculated for each material as the RSD of the individual

mass fraction measurement results) ranging from about 2% to 54%. For ten of the RMs measured the RSD is <20%, whilst five have >30% RSDs of the mean. This suggests that mass fraction measurements made during MC-ICP-MS isotopic analyses may be suitable for assessing sample heterogeneity. Importantly, there was no resolvable variation of Tl mass fraction with digestion method: for materials analysed following both hotplate and bomb digestion, Tl mass fraction RSDs are <15% (see also Figure 3). This strongly suggests that Tl is not hosted in refractory phases present in these RMs.

**Comparison with literature data:** Jochum *et al.* (2016) provide GeoReM preferred values for the 19 most frequently queried RMs, including AGV-2, BCR-2, BHVO-2 and G-2. Additional literature reports of Tl mass fraction exist for Mica-Fe, BCR-2, GSP-2, G-2, STM-1, and UB-N. These values are reported in Table 4 alongside the mass fraction results obtained over the course of this study. Only the mass fractions determined for GSP-2 and STM-1 differ significantly from published values.

For AL-I, AN-G, and Mica-Mg only proposed values are available, from the compilation of Govindaraju (1995). No Tl mass fraction estimates are available for COQ-1, trachytes ISH-G and MDO-G, or K-feldspars FK-N and NIST SRM 607. To the best of our knowledge, we provide the first reported values for these reference materials.

Good agreement between literature reports of Tl mass fractions in these materials and our results, particularly for well-characterised RMs, provide reassurance that the BHVO-2 digestions used as calibrator did not exhibit anomalously high Tl mass fractions. We are confident that the mass fraction data presented are robust.

*Determination of Tl isotope ratios*

**Blanks and Reference Solutions:** Due to the low mass fraction of Tl (typically 10s ng $g^{-1}$) in many rock samples (Table 4), it is necessary that Tl mass fractions of total procedural blanks are below the detection limit of the MC-ICP-MS. This equates to a maximum of 2 pg Tl, where the smallest amount of sample Tl processed was approximately 2.5 ng (for AN-G). The total procedural Tl blank for each batch of samples was determined by dissolving the total procedural blank in 1ml of analysis solution (0.1 mol $l^{-1}$ $HNO_3$–0.1% $H_2SO_4$) and monitoring the intensity of the m/z 205 ion beam. In all cases there was no deviation of the signal from the wash background, indicative of a maximum blank of <1 pg.

Residual Pb can produce significant errors in the measured $^{208}Pb/^{206}Pb$ isotope ratio used for correction of mass bias. Thus, any Pb present in the sample solution prior to addition of SRM 981, whether residual from the sample matrix or introduced via contamination, has the potential to affect the precision and repeatability of $\varepsilon^{205}Tl_{SRM997}$ measurements. Therefore, to ensure accuracy of measured $\varepsilon^{205}Tl_{SRM997}$, residual Pb mass fractions of below 0.01 ng $g^{-1}$ were required for every sample solution and for the total procedural blank, as determined from the observed m/z 208 ion beam signal prior to SRM 981 addition. Typical residual Pb mass fractions were approximately equivalent to 1 pg $g^{-1}$.

Over the course of this study, over 200 measurement results of the Aldrich Tl solution yield a mean $\varepsilon^{205}Tl_{SRM997}$ value of -0.8 ± 0.3 (2*s* , n = 211; Figure 4), in excellent agreement with the most recent compilation of data from seven laboratories worldwide (Nielsen *et al.* 2017) in which the value is given as $\varepsilon^{205}Tl_{SRM997}$ = -0.79 ± 0.35 (2*s*, n = 187). Due to the large number of analyses, our intermediate precision (2*s*) is calculated using the average $\varepsilon^{205}Tl_{SRM997}$ values obtained for the Aldrich Tl solution during each analytical session.

**Data quality:** Results for the Tl isotope ratio measurements are given in Table 5. As a minimum of 3 isotope ratio measurements were made for each RM, the reported intermediate precision (2*s*) is based on at least three measurement results obtained following independent sample preparation. For comparison, the typical external reproducibility for multiple digestions performed in multiple instituions of $\varepsilon^{205}Tl_{SRM997}$ for geological samples is ±0.5 *ε*-units (see compilation in Nielsen *et al*. 2017).

Literature reports of $\varepsilon^{205}Tl_{SRM997}$ exist for AGV-2, BCR-2, BHVO-2 and G-2 (Table 1). Of these, BCR-2 has the most widely-reported $\varepsilon^{205}Tl_{SRM997}$, and can be considered isotopically homogeneous with respect to Tl isotope ratio. The values we obtain for BCR-2 and BHVO-2 are in excellent accord with Prytulak *et al.* (2013, 2017) and Coggon *et al.* (2014), and are indistinguishable from values obtained by Baker *et al.* (2009).

However, the value we obtain for G-2 is in disagreement with the single previously reported value (Rehkämper and Halliday 1999), in spite of large variance for both measurements. The low precisions and difference in isotope ratio measurement results most likely arise from (i) G-2 exhibiting powder heterogeneity in terms of Tl (see subsequent discussion), (ii) analysis of different bottles of G-2, and (c) difficulties with development of the techniques for isotopic analysis of Tl.

We are therefore confident that the measurement procedure employed has not introduced any systematic bias, and that our $\varepsilon^{205}Tl_{SRM997}$ values and precisions for previously uncharacterised RMs provide a range where the true value is likely to be. Together with mass fraction measurement results obtained via MC-ICP-MS on the same dissolution, these Tl isotope ratio results are displayed in Figure 3, as mean values for each individual dissolution. There is no correlation of precision with digestion batch or analytical sessions, implying that the better precisions (2*s* = 0.4-0.6 *ε*-units) are representative of the precision achievable with this analytic approach, whilst the higher measurement results with lower precision (up to 2 *ε*-units) are unlikely to be a consequence of our laboratory techniques or poor measurement precision.

**Evaluation of reference material heterogeneity:** Despite the demonstrated ability of the analytical techniques to achieve excellent precision, the variances for some samples are surprisingly high, suggesting possible isotopic heterogeneity in the RM powders. Reference materials must be homogeneous in the element system of interest if they are to be used for method development, validation, or interlaboratory comparisons (BIPM et al. 2012). Homogeneity is routinely tested for major elements and some trace elements during RM preparation but heterogeneity for other elements and for isotope systems has been identified in a number of these materials (e.g. BHVO-2: Baker *et* al. 2004, Weis *et al.* 2006, Chauvel *et al.* 2011; SRM 607: Nebel and Mezger 2006). Furthermore, the statistical nature of observed heterogeneity can provide information on the dispersal of an enriched phase or phases through a material. For example, Chauvel *et al.* (2011) discuss the possibility that relatively large, rare Pb-rich microparticles are responsible for the distinctive bimodal distribution of Pb mass fractions in BHVO-2. However, we are not aware of any general assessment of Tl heterogeneity in igneous RMs.

As $Tl^+$ readily substitutes for $K^+$ in igneous minerals, it is expected that, if present, K-rich phases will dominate the Tl budget of a rock. Indeed, as shown in Figure 5 for silicate rocks Tl mass fraction correlates with $K_2O$. Figure 3 presents mean $\varepsilon^{205}Tl_{SRM997}$ and mass fraction values obtained using MC-ICP-MS for each RM and for each individual dissolution, to aid qualitative assessment of any Tl heterogeneities. There are no resolvable differences in either Tl mass fractions or isotope ratios between bomb and hotplate digestions for the RMs studied, providing evidence that Tl is not hosted in refractory phases. Thus small variations in the proportions of K-rich phases in the powder portion sampled could significantly affect both the mass fraction and isotope ratio of Tl.

Having performed a minimum of three digestions for isotope ratio measurement of each RM included in this study, we are able to assess whether these materials are heterogeneous for Tl. Examination of the dataset (Figure 3) reveals heterogeneity of mass fraction with weak or no isotope ratio heterogeneity for COQ-1, STM-1, AN-G and Mica-Mg, marked heterogeneity of both isotope ratio and mass fraction for G-2, and possible weak isotope ratio heterogeneity for BHVO-2.

AN-G consists primarily of anorthosite ($An_{80}$-$An_{85}$), with hornblende (10-15 % v/v), relict clinopyroxene, and some secondary minerals (Govindaraju 1980). In this rock hornblendes are likely the major host of K and therefore of Tl; if the hornblendes have identical Tl isotope ratios to the rest of the bulk sample, it follows that Tl isotope ratios will be unaffected by modal proportion of hornblende in any individual dissolution, but the Tl mass fraction will be strongly dependent on the amount of hornblende incorporated into the digested portion. STM-1 contains multiple K-bearing phases including alkali feldspar, nepheline and biotite (Snavely *et al.* 1976), and features a bulk Tl mass fraction two orders of magnitude higher than AN-G. On the basis of three dissolutions, STM-1 appears to exhibit a bimodal distribution for Tl: two distinct mass fraction populations, with the higher mass fraction possibly weakly associated with an isotopically lighter $\varepsilon^{205}Tl_{SRM997}$ signature. This may reflect the existence of at least two distinct hosts of Tl, variably incorporated into the sample portion. In contrast, across four dissolutions Mica-Mg appears to display a range in both Tl mass fraction and $\varepsilon^{205}Tl_{SRM997}$, with no clear systematics; this is consistent with relatively small, frequent microparticles of several Tl-rich and isotopically distinct phases unevenly dispersed throughout the powdered RM.

G-2 appears to exhibit significant heterogeneities in Tl mass fraction and isotope ratio. As with STM-1, these heterogeneities appear to be weakly coupled. G-2 is a micaceous granite, known to contain microcline, biotite and muscovite (Fairbairn *et al.* 1951, Chayes and Suzuki 1963, Flanagan 1969). These K-rich phases are likely to be the major hosts of Tl in G-2; given the difficulty of ensuring even crushing and even distribution of sheet silicates, it is plausible that small variations in the amount of each phase sampled in any given digestion could account for the coupled heterogeneity seen here.

Petrographic information is not available for BHVO-2, but as a basalt, it is unlikely to contain significant amounts of K-rich phases. We do not observe any evidence for the significant Tl mass fraction variations reported in the literature (Appendix 1), but do see potential evidence of weak Tl isotope ratio heterogeneity.

Constraints on the scale of isotope ratio heterogeneities are provided by a comparison of dissolved mass versus the 2*s* precision of the measurement result of $\varepsilon^{205}Tl_{SRM997}$ (Figure 6). For samples with higher (known or predicted) Tl mass fractions, smaller masses were digested to yield similar amounts of Tl for measurement. However, it is precisely the samples with high Tl contents and low digested mass that, in general, display the largest variance in the isotope ratio measurements. For most RMs included in this study it appears that weighing out at minimum 100mg of powder might mitigate the effects of small-scale heterogeneity and enable routinely achievable $\varepsilon^{205}Tl_{SRM997}$ measurements with 2*s* precisions on the order of 0.5 $\varepsilon$-units.

However, it is unlikely that dissolving larger initial masses would improve the precisions achievable for G-2 and BHVO-2; G-2 in particular exhibits a high variance given initial dissolved masses, suggesting that the discrepancy with the one previous report (Rehkämper and Halliday 1999) arises in large part from powder heterogeneity. Rehkämper and Halliday (1999) are known to have made their analysis using a different vial of G-2, potentially indicating heterogeneity between vials. We therefore recommend against use of G-2 as a Tl reference material. For BHVO-2 the variance for $\varepsilon^{205}Tl_{SRM997}$ is less extreme and, unlike G-2, there is no strong evidence for heterogeneity in Tl mass fraction. We therefore recommend caution when employing BHVO-2 as a Tl isotope reference material, but as it is the only basaltic RM with a Tl mass fraction of ~20 ng $g^{-1}$, we recognise that it is likely the most appropriate choice for studies involving low-Tl igneous samples. As BHVO-1 and BHVO-2 are distinctly different in terms of both mass fraction and isotope ratio values (Appendix 1, Table 1), care must be taken to ensure that these materials are not confused if using either as a reference material.

In light of concerns regarding potential inhomogeneous contamination during the generation of RMs, we find no evidence that the overall reported range in $\varepsilon^{205}Tl_{SRM997}$ for the RMs analysed here (5.5 $\varepsilon$-units, comparable to that of other natural igneous products: see Nielsen *et al.* 2017) is due to

contamination of the samples. In particular, there is no systematic variation of Tl isotope composition with RM provider or date of preparation. Furthermore, the most isotopically distinct result (serpentinite UB-N: $\varepsilon^{205}Tl_{SRM997}$ = +1.8 ± 0.4 2*s*) is consistent with the findings of Nielsen *et al.* (2015). To the best of our knowledge these authors provide the only literature report of $\varepsilon^{205}Tl_{SRM997}$ in natural serpentinite samples, and these show similarly heavy Tl isotope compositions, providing indirect validation of our isotopically heavy serpentinite RM.

# SUMMARY

Thallium mass fraction and isotope ratio measurements were performed for a comprehensive suite of sixteen geological reference materials, including both bulk rock and partially-separated mineral powders. We provide the first reported Tl mass fraction and $\varepsilon^{205}Tl_{SRM997}$ (i.e. $\delta^{205}Tl_{SRM997}$ in parts per ten thousand) measurement results for geochemical reference materials 14P, Albite AL-I, Anorthosite AN-G, Carbonatite COQ-1, Potash Feldspar FK-N, Trachyte ISH-G, Trachyte MDO-G, and Phlogopite Mica-Mg; and additionally provide the first reported $\varepsilon^{205}Tl_{SRM997}$ values for Biotite Mica-Fe and Serpentinite UB-N.

Of the 16 reference materials included, all but G-2 are in principle appropriate for use as Tl isotopic reference materials, provided sufficiently large test portion sizes (minimum 100mg) are chosen for digestion. The $\varepsilon^{205}Tl_{SRM997}$ represented spans from -3.5 to +1.8, comparable to the range thus far reported in global igneous rocks (e.g. Nielsen *et al.* 2017).

# ACKNOWLEDGEMENTS

AB was supported by a Janet Watson Earth Science and Engineering Departmental PhD studentship. B. Coles and K. Kreissig are gratefully acknowledged for maintenance of the MAGIC mass spectrometry and clean lab facilities. We thank M. Mangler, B. Mitchell-Bunce, S. Munson,

656 and F. Wei for contributions to RM digestion at Imperial for trace element analyses, and B. Charlier
657 for providing the NIST SRM 607 reference material. We gratefully acknowledge the comments of
658 two anonymous reviewers and the editor, Thomas Meisel, which have improved the text.

# REFERENCES


Anders E. and Stevens C.M. (1960) Thallium-205 and the age of the solar system. **Journal of Geophysical Research, 65,** 2471-2472.

Andreasen R., Schönbächler M. and Rehkämper M. (2009) The 205Pb-205Tl and Cd isotope systematics of ordinary chondrites. **Geochimica et Cosmochimica Acta, 73,** A43-A43.

Andreasen R., Rehkämper M., Benedix G.K., Theis K.J., Schönbächler M. and Smith C.L. (2012) Lead-thallium chronology of IIAB and IIIAB iron meteorites and the solar system initial abundance of lead-205. 43rd Lunar and Planetary Science Conference**,** Abstract 2902.

Arden J.W. (1983) Distribution of lead and thallium in the matrix of the Allende meteorite and the extent of terrestrial lead contamination in chondrites. **Earth and Planetary Science Letters, 62,** 395-406.

Babechuk M.G., Kamber B.S., Greig A., Canil D. and Kodolányi J. (2010) The behaviour of tungsten during mantle melting revisited with implications for planetary differentiation time scales. **Geochimica et Cosmochimica Acta**, **74,** 1448-1470.

Babechuk M.G. and Kamber B.S. (2011) An estimate of 1.9 Ga mantle depletion using the high-field-strength elements and Nd–Pb isotopes of ocean floor basalts, Flin Flon Belt, Canada. **Precambrian Research, 189,** 114-139.

Baker J., Peate D., Waight T. and Meyzen C. (2004) Pb isotopic analysis of standards and samples using a $^{207}Pb$–$^{204}Pb$ double spike and thallium to correct for mass bias with a double-focusing MC-ICP-MS. **Chemical Geology, 211,** 275-303.

Baker R.G.A., Rehkämper M., Hinkley T.K., Nielsen S.G. and Toutain J.P. (2009) Investigation of thallium fluxes from subaerial volcanism—Implications for the present and past mass balance of thallium in the oceans. **Geochimica et Cosmochimica Acta, 73,** 6340-6359.

Baker R.G.A., Rehkämper M., Ihenfeld C., Oates C.J. and Coggon R. (2010a) Thallium isotope variations in an ore-bearing continental igneous setting: Collahusasi Formation, northern Chile.

685 **Geochimica et Cosmochimica Acta, 73,** 4405-4416.

686 Baker R.G.A., Schönbächler M., Rehkämper M., Williams H.M. and Halliday A.N. (2010b) The
687 thallium isotope composition of carbonaceous chondrites - new evidence for live Pb-205 in the
688 early solar system. **Earth and Planetary Science Letters, 291,** 39-47.

689 Balaram V. and Rao T.G. (2003) Rapid determination of REEs and other trace elements in
690 geological samples by microwave acid digestion and ICP-MS. **Atomic Spectroscopy, 24,** 206-
691 212.

692 Baranov B.V., Werner R., Hoernle K.A., Tsoy I.B., van den Bogaard P. and Tararin I.A. (2002)
693 Evidence for compressionally induced high subsidence rates in the Kurile Basin (Okhotsk Sea).
694 **Tectonophysics, 350,** 63-97.

695 Barnes J.D., Beltrando M., Lee Cin-Ty Aeolus, Cisneros M., Loewy S., Chin E. (2014)
696 Geochemistry of Alpine serpentinites from rifting to subduction: a view across paleogeographic
697 domains and metamorphic grade. **Chemical Geology, 389,** 29-47.

698 Bately G.E. and Florence T.M. (1975) Determination of thallium in natural waters by anodic
699 stripping voltammetry. **Journal of Electroanalytical Chemistry and Interfacial Electrochemist,**
700 **61,** 205–211.

701 Bigeleisen J. and Mayer M.G. (1947) Calculation of equilibrium constants for isotopic exchange
702 reactions. **Journal of Chemical Physics, 15,** 261-267.

703 BIPM, IEC, IFCC, ILAC, IUPAC, IUPAP, ISO, OIML (2012) The international vocabulary of
704 metrology—basic and general concepts and associated terms (VIM), 3rd edn. JCGM 200:2012.

705 Bolge L.L., Carr M.J., Feigenson M.D. and Alvarado G.E. (2006) Geochemical stratigraphy and
706 magmatic evolution at Arenal Volcano, Costa Rica. **Journal of Volcanology and Geothermal**
707 **Research, 157,** 34-48.

708 Bouman C., Elliot T. and Vroon P.Z. (2004) Lithium inputs to subduction zones. **Chemical**
709 **Geology, 212,** 59-79.

710 Brandl P.A., Beier C., Regelous M., Abouchami W., Haase K.M., Garbe-Schönberg D. and Galer

S.J.G. (2012) Volcanism on the flanks of the East Pacific Rise: quantitative constraints on mantle heterogeneity and melting processes. **Chemical Geology, 298-299,** 41-56.

Brown R.J.C. and Milton M.J.T. (2005) Analytical techniques for trace element analysis: an overview. **Trends in Analytical Chemistry, 24,** 266-274.

Chauvel C., Bureau S. and Poggi C. (2011) Comprehensive chemical and isotopic analyses of basalt and sediment reference materials. **Geostandards and Geoanalytical Research, 35,** 125-143.

Chauvel C., Maury R.C., Blais S., Lewin E., Guillou H., Guille G., Rossi P. and Gutscher M.-A. (2012) The size of plume heterogeneities constrained by Marquesas isotopic stripes. **Geochemistry Geophysics Geosystems, 13,** Q07005, 23pp. 10.1029/2012GC004123.

Chayes F. and Suzuki Y. (1963) A replacement for reference sample G-l. **In: Carnegie Institute Washington, Annual report of the Director of the Geophysical Laboratory, 62,** 155-156.

Chen J.H. and Wasserburg G.J. (1987) A search for evidence of extinct lead-205 in iron meteorites. 18th Lunar and Planetary Science Conference, Abstract 1084.

Chen J.H. and Wasserburg G.J. (1994) The abundance of thallium and primordial lead in selected meteorites - the search for $^{205}$Pb. 25th Lunar and Planetary Science Conference, Abstract 1105.

Coggon R.M., Rehkämper M., Atteck C., Teagle D.A.H., Alt J.C. and Cooper M.J. (2014) Controls on thallium uptake during hydrothermal alteration of the upper ocean crust. **Geochimica et Cosmochimica Acta, 144,** 25-42.

Condomines M., Carpentier M. and Ongendangenda T. (2015) Extreme radium deficit in the 1957 AD Mugogo lava (Virunga volcanic field, Africa): its bearing on olivine-melilitite genesis. **Contributions to Mineralogy and Petrology, 169:29** 19pp. 10.1007/s00410-015-1124-9.

Crookes W. (1862) Preliminary researches on thallium. **Proceedings of the Royal Society of London, 12,** 150-159.

Coplen, T.B. Guidelines and recommended terms for expression of stable-isotope-ratio and gas-ratio measurement results. (2011) **Rapid Communications in Mass Spectrometry, 25, 2538-2560.**

737 Croudace I.W. (1980) A possible error source in silicate wet chemistry caused by insoluble
738 fluorides. **Chemical Geology, 31,** 153-155.

739 Dampare S.B., Shibata T., Asiedu D.K., Osae S. and Banoeng-Yakubo B. (2008) Geochemistry of
740 Paleoproterozoic metavolcanic rocks from the southern Ashanti volcanic belt, Ghana: Petrogenetic
741 and tectonic setting implications. **Precambrian Research, 162,** 403-423.

742 Deegan F.M., Troll V.R., Barker A.K., Harris C., Chadwick J.P., Carracedo J.C. and Delcamp A.
743 (2012) Crustal versus source processes recorded in dykes from the Northeast volcanic rift zone of
744 Tenerife, Canary Islands. **Chemical Geology, 344,** 324-344.

745 Deng H., Kusky T., Polat A., Wang L., Wang J. and Wang S. (2013) Geochemistry of Neoarchean
746 mafic volcanic rocks and late mafic dikes in the Zanhuang Complex, Central Orogenic Belt, North
747 China Craton: implications for geodynamic setting. **Lithos, 175-176,** 193-212.

748 Eggins S.M., Woodhead J.D., Kinsley L.P.J., Mortimer G.E., Sylvester P., McCulloch M.P., Hergt
749 J.M. and Handler M.R. (1997) A simple method for the precise determination of ≥ 40 trace
750 elements in geological samples by ICPMS using enriched isotope internal standardisation.
751 **Chemical Geology, 134,** 311-326.

752 Elmaleh A., Galy A., Allard T., Dairon R., Day J.A., Michel F., Marriner N., Morhange C. and
753 Couffignal F. (2012) Anthropogenic accumulation of metals and metalloids in carbonate-rich
754 sediments: Insights from the ancient harbor setting of Tyre (Lebanon). **Geochimica et**
755 **Cosmochimica Acta, 82,** 23-38.

756 Espanon V.R., Chivas A.R., Kinsley L.P.J. and Dosseto A. (2014) Geochemical variations in the
757 Quaternary Andean back-arc volcanism, southern Mendoza, Argentina. **Lithos, 208-209,** 251-264.

758 Fairbairn H.W., Schlecht W.G., Stevens R.E., Dennen W.H., Ahrens L.H. and Chayes F. (1951) A
759 cooperative investigation of precision and accuracy in chemical, spectrochemical and modal
760 analysis of silicate rocks. **Geological Survey Bulletin, 980**, 59.

761 Flanagan F.J. (1967) US Geological Survey silicate rock standards. **Geochimica et Cosmochimica**
762 **Acta, 31,** 289-308.

763 Flanagan F.J. (1969) U.S. Geological Survey standards—II. First compilation of data for the new
764 U.S.G.S. rocks. **Geochimica et Cosmochimica Acta, 33,** 81-120.

765 Flanagan F.J. and Carroll G.V. (1976) Mica schist, SDC-1, from Rock Creek Park, Washington,
766 D.C. **In: Flanagan F.J. (ed), Descriptions and analyses of eight new USGS rock standards,**
767 **United States, Geological Survey, Professional Paper, 840,** 29-32.

768 Flanagan F.J., Wright T.L., Taylor S.R., Annell C.S., Christian R.C. and Dinnin J.I. (1976) Basalt,
769 BHVO-1, from Kilauea Crater, Hawaii. **In: Flanagan F.J. (ed), Descriptions and analyses of**
770 **eight new USGS rock standards, United States, Geological Survey, Professional Paper, 840,**
771 33-39.

772 Fretzdorff S., Livermore R.A., Devey C.W., Leat P.T. and Stoffers P. (2002) Petrogenesis of the
773 back-arc East Scotia Ridge, South Atlantic Ocean. **Journal of Petrology, 43,** 1435-1467.

774 Fujii Y., Nomura M., Okamoto M., Onitsuka H., Kawakami F. and Takeda K. (1989a) An
775 anomalous isotope effect of U-235 in U(IV)-U(VI) chemical exchange. **Zeitschrift Für**
776 **Naturforschung Section a-a Journal of Physical Sciences, 44**, 395-398.

777 Fujii Y., Nomura M., Onitsuka H. and Takeda K. (1989b) Anomalous isotope fractionation in
778 uranium enrichment process. **Journal of Nuclear Science and Technology, 26,** 1061-1064.

779 Fujii T., Moynier F., Agranier A., Ponzevera E., Abe M., Uehara A. and Yamana H. (2013) Nuclear
780 field shift effect in isotope fractionation of thallium. **Journal of Radioanalytical and Nuclear**
781 **Chemistry, 296,** 261-265.

782 Gale A., Escrig S., Gier E.J., Langmuir C.H. and Goldstein S.J. (2011) Enriched basalts at segment
783 centers: The Lucky Strike (37°17′N) and Menez Gwen (37°50′N) segments of the Mid-Atlantic
784 Ridge. **Geochemistry Geophysics Geosystems, 12,** Q06016, 26pp. 10.1029/2010GC003446.

785 Garbe-Schönberg C.-D. (1993) Simultaneous determination of thirty-seven trace elements in
786 twenty-eight international rock standards by ICP-MS. **Geostandards Newsletter, 17,** 81-97.

787 Gaschnig R.M., Rudnik R.L. and McDonough W.F. (2015) Determination of Ga, Ge, Mo, Ag, Cd,
788 In, Sn, Sb, W, Tl and Bi in USGS reference materials by standard addition ICP-MS.

**Geostandards and Geoanalytical Research, 39,** 371-379.

Geldmacher J., Hoernle K.A., van den Bogaard P., Hauff F. and Klügel A. (2008) Age and geochemistry of the Central American Forearc Basement (DSDP Leg 67 and 84): insights into Mesozoic arc volcanism and seamount accretion on the fringe of the Caribbean LIP. **Journal of Petrology, 49,** 1781-1815.

Gibson S.A., McMahon S.C., Day J.A. and Dawson J.B. (2013) Highly refractory lithospheric mantle beneath the Tanzanian Craton: evidence from Lashaine pre-metasomatic garnet-bearing peridotites. **Journal of Petrology, 54,** 1503-1546.

Gillot P.-Y., Cornette Y., Max N. and Floris B. (1992) Two reference materials, trachytes MDO-G and ISH-G, for argon dating (K-Ar and $^{40}Ar/^{39}Ar$) of Pleistocene and Holocene rocks. **Geostandards Newsletter, 16,** 55-60.

Gómez-Tuena A., LaGatta A. B., Langmuir C.H., Goldstein S.L., Ortega-Gutiérrez F. and Carrasco-Núñez G. (2003) Temporal control of subduction magmatism in the eastern Trans-Mexican Volcanic Belt: mantle sources, slab contributions, and crustal contamination. **Geochemistry Geophysics Geosystems, 4,** 8912, 33pp. 10.1029/2003GC000524.

Gómez-Tuena A., Mori L., Goldstein S.L. and Pérez-Arvizu O. (2011) Magmatic diversity of western Mexico as a function of metamorphic transformations in the subducted oceanic plate. **Geochimica et Cosmochimica Acta, 75,** 213-241.

González-Álvarez I. and Kerrich R. (2011) Trace element mobility in dolomitic argillites of the Mesoproterozoic Belt-Purcell Supergroup, Western North America. **Geochimica et Cosmochimica Acta, 75,** 1733-1756.

Govindaraju K. (1979) Report (1968-1978) on two mica reference samples: Biotite Mica-Fe and Phlogopite Mica-Mg. **Geostandards Newsletter, 3,** 3-24.

Govindaraju K. (1980) Report (1980) on three GIT-IWG rock reference samples: anorthosite from Greenland, AN-G; Basalte d'Essay-la-Côte, BE-N; Granite de Beauvoir, MA-N. **Geostandards Newsletter, 4,** 49-138.

Govindaraju K. (1982) Report (1967-1981) on four ANRT rock reference samples: Diorite DR-N,

816 Serpentine UB-N, Bauxite BX-N and Disthene DT-N. **Geostandards Newsletter, 6,** 91-159.

817 Govindaraju K. (1984a) Report (1984) on two GIT-IWG geochemical reference samples: albite
818 from Italy, AL-I and iron formation sample from Greenland, IF-G. **Geostandards Newsletter, 8,**
819 63-113.

820 Govindaraju K. (1984b) Report (1973-1984) on two ANRT geochemical reference samples: Granite
821 GS-N and Potash Feldspar FK-N. **Geostandards Newsletter, 8,** 173-206.

822 Govindaraju K. and Roelandts I. (1988) Compilation report (1966-1987) on trace elements in five
823 CRPG geochemical reference samples: basalt BR; granites, GA and GH; micas, biotite Mica-Fe
824 and phlogopite Mica-Mg. **Geostandards Newsletter, 12,** 119-201.

825 Govindaraju K. (1994) 1994 compilation of working values and sample description for 383
826 geostandards. **Geostandards Newsletter, 18,** 1-158.

827 Govindaraju K. (1995) 1995 working values with confidence limits for twenty-six CRPG, ANRT
828 and IWG-GIT geostandards. **Geostandards Newsletter, 19,** 1-32.

829 He Y., Zhao G., Sun M. and Han Y. (2010) Petrogenesis and tectonic setting of volcanic rocks in
830 the Xiaoshan and Waifangshan areas along the southern margin of the North China Craton:
831 Constraints from bulk-rock geochemistry and Sr–Nd isotopic composition. **Lithos, 114,** 186-199.

832 Heinrich E.W. (1960) Kingman feldspar mine. **Arizona Bureau of Mines, 167,** 5-11.

833 Hergt J., Woodhead J. and Schofield A. (2007) A-type magmatism in the Western Lachlan Fold
834 Belt? A study of granites and rhyolites from the Grampians region, Western Victoria. **Lithos, 97,**
835 122-139.

836 Hettmann K., Marks M.A.W., Kreissig K., Zack T., Wenzel T., Rehkämper M., Jacob D.E. and
837 Markl G. (2014) The geochemistry of Tl and its isotopes during magmatic and hydrothermal
838 processes: the peralkaline Ilimaussaq complex, southwest Greenland. **Chemical Geology, 366,** 1-
839 13.

840 Horne R.A. (1958) The ion-exchange resin adsorption of thallium(I) and (III). **Journal of**
841 **Inorganic and Nuclear Chemistry, 6,** 338-343.

842 Hu Z. and Gao S. (2008) Upper crustal abundances of trace elements: a revision and update.
843 **Chemical Geology, 253,** 205-221.

844 Hu Z., Zhang W., Liu Y., Chen H., Gaschnig R.M., Zong K., Li M., Gao S. and Hu S. (2013) Rapid
845 bulk rock decomposition by ammonium fluoride (NH4F) in open vessels at an elevated digestion
846 temperature. **Chemical Geology, 355,** 144-152.

847 Huey J.M. and Kohman T.P. (1972) Search for extinct natural radioactivity of $^{205}$Pb via thallium-
848 isotope anomalies in chondrites and lunar soil. **Earth and Planetary Science Letters, 16,** 401-
849 412.

850 Jacques G., Hoernle K., Gill J., Hauff F., Wehrmann H., Garbe-Schönberg D., van den Bogaard P.,
851 Bindeman I. and Lara L.E. (2013) Across-arc geochemical variations in the Southern Volcanic
852 Zone, Chile (34.5–38.0°S): constraints on mantle wedge and slab input compositions. **Geochimica**
853 **et Cosmochimica Acta, 123,** 218-243.

854 Jochum K.P., Nohl U., Herwig K., Lammel E., Stoll B. and Hofmann A.W. (2005) GeoReM: a new
855 geochemical database for reference materials and isotopic standards. **Geostandards and**
856 **Geoanalytical Research, 29,** 333-338.

857 Jochum K.P., Weis U., Schwager B., Stoll B., Wilson S.A., Haug G.H., Andreae M.O. and
858 Enzweiler J. (2016) Reference values following ISO guidelines for frequently requested rock
859 reference materials. **Geostandards and Geoanalytical Research, 40,** 333-350.

860 Kamber B.S., Greig A. and Collerson K.D. (2005) A new estimate for the composition of weathered
861 young upper continental crust from alluvial sediments, Queensland, Australia. **Geochimica et**
862 **Cosmochimica Acta, 69,** 1041-1058.

863 Kawabata H., Hanyu T., Chang Q., Kimura J.-I., Nichols A.R.L and Tatsumi Y. (2011) The
864 petrology and geochemistry of St Helena alkali basalts: evaluation of the oceanic crust-recycling
865 model for HIMU OIB. **Journal of Petrology, 52,** 791-838.

866 Kersten M., Xiao T., Kreissig K., Brett A., Coles B.J., and Rehkämper M. (2014) Tracing
867 anthropogenic thallium in soil using stable isotope compositions. **Environmental Science &**

**Technology, 48,** 9030-9036.

King W.H. (1984) Isotope shifts in atomic spectra. **Plenum Press (New York),** 210pp.

Kersten M., Xiao T., Kreissig K., Brett A., Coles B.J., and Rehkämper M. (2014) Tracing anthropogenic thallium in soil using stable isotope compositions. Environmental Science & Technology, 48, 9030-9036.

Kirchenbaur M., Münster C., Schuth S., Garbe-Schönberg D. and Marchev P. (2012) Tectonomagmatic constraints on the sources of Eastern Mediterranean K-rich lavas. **Journal of Petrology, 53,** 27-65.

Knesel K.M. and Duffield W.A. (2007) Gradients in silicic eruptions caused by rapid inputs from above and below rather than protrated chamber differentiation. **Journal of Volcanology and Geothermal Research, 167,** 181-197.

Kodolányi J., Pettke T., Spandler C., Kamber B.S. and Gméling K. (2012) Geochemistry of ocean floor and fore-arc serpentinites: Constraints on the ultramafic input to subduction zones. **Journal of Petrology, 53,** 235-270.

Korotev R.L. (1996) A self-consistent compilation of elemental concentration data for 93 geochemical reference samples. **Geostandards and Geoanalytical Research, 20,** 217-245.

Kraus K.A., Nelson F. and Smith G.W. (1954) Anion-exchange studies. IX. Adsorbability of a number of metals in hydrochloric acid solutions. **Journal of Physical Chemistry, 58,** 11-17.

Lackschewitz K.S., Singer A., Botz R., Garbe-Schönberg D., Stoffers P. and Horz K. (2000) Formation and transformation of clay minerals in the hydrothermal deposits of Middle Valley, Juan de Fuca Ridge, ODP Leg 169. **Economic Geology, 95,** 361-390.

Lamy C.-A. (1862) De l'existence d'un nouveau métal, le thallium. **Comptes rendus, 54,** 1255-1258.

Lee C.-T.A., Yin Q.-z., Lenardic A., Argranier A., O'Neill C.J. and Thiagarajan N. (2007) Trace-element composition of Fe-rich residual liquids formed by fractional crystallization: Implications for the Hadean magma ocean. **Geochimica et Cosmochimica Acta, 71,** 3601-3615.

894 Makishima A. and Nakamura E. (2006) Determination of major, minor and trace elements in
895 silicate samples by ICP-QMS and ICP-SFMS applying isotope dilution-internal standardization
896 (ID-IS) and multi-stage internal standardization. **Geostandards and Geoanalytical Research, 30,**
897 245-271.

898 Makishima A., Kitagawa H. and Nakamura E. (2011) Simultaneous determination of Cd, In, Tl and
899 Bi by isotope dilution-internal standardization ICP-QMS with corrections using externally
900 measured $MoO^+/Mo^+$ ratios. **Geostandards and Geoanalytical Research, 35,** 57-67.

901 Martin A.P., Price R.C., Cooper A.F. and McCammon C. (2015) Petrogenesis of the rifted Southern
902 Victoria Land lithospheric mantle, Antarctica, inferred from petrography, geochemistry,
903 thermobarometry and oxybarometry of peridotite and pyroxenite xenoliths from the Mount
904 Morning eruptive centre. **Journal of Petrology, 56,** 193-226.

905 Marx S.K. and Kamber B.S. (2010) Trace-element systematics of sediments in the Murray–Darling
906 Basin, Australia: Sediment provenance and palaeoclimate implications of fine scale chemical
907 heterogeneity. **Applied Geochemistry, 25,** 1221-1237.

908 Marx S.K., Kamber B.S., McGowan H.A. and Zawadski A. (2010) Atmospheric pollutants in alpine
909 peat bogs record a detailed chronology of industrial and agricultural development on the
910 Australian continent. **Environmental Pollution, 158,** 1615-1628.

911 McCoy-West A.J., Baker J.A., Faure K. and Wysoczanski R.J. (2010) Petrogenesis and origins of
912 mid-cretaceous continental intraplate volcanism in Marlborough, New Zealand: implications for
913 the long-lived HIMU magmatic mega-province of the SW Pacific. **Journal of Petrology, 51,**
914 2003-2045.

915 Mohan M.R., Piercey S.J., Kamber B.S. and Sarma D.S. (2013) Subduction related tectonic
916 evolution of the Neoarchean eastern Dharwar Craton, southern India: new geochemical and
917 isotopic constraints. **Precambrian Research, 227,** 204-226.

918 Mori L., Gómez-Tuena A., Cai Y. and Goldstein S.L. (2007) Effects of prolonged flat subduction
919 on the Miocene magmatic record of the central Trans-Mexican Volcanic Belt. **Chemical Geology,**
920 **244,** 452-473.

921 Mori L., Gómez-Tuena A., Schaaf P., Goldstein S.L., Pérez-Arvizu O. and Solís-Pichardo G.
922 (2009) Lithospheric removal as a trigger for flood basalt magmatism in the Trans-Mexican
923 Volcanic Belt. **Journal of Petrology, 50,** 2157-2186.

924 Moune S., Gauthier P.-J., Gislason S.R. and Sigmarsson O. (2006) Trace element degassing and
925 enrichment in the eruptive plume of the 2000 eruption of Hekla volcano, Iceland. **Geochimica et**
926 **Cosmochimica Acta, 70,** 461-479.

927 Moynier F., Fujii T., Brennecka G.A. and Nielsen S.G. (2013) Nuclear field shift in natural
928 environments. **Comptes Rendus Geoscience, 345,** 150-159.

929 Nebel O. and Mezger K. (2006) Reassessment of the NBS SRM-607 K-feldspar as a high precision
930 Rb/Sr and Sr isotope reference. **Chemical Geology, 233**, 337-345.

931 Nielsen S.G., Rehkämper M., Baker J. and Halliday A.N. (2004) The precise and accurate
932 determination of thallium isotope compositions and concentrations for water samples by MC-
933 ICPMS. **Chemical Geology, 204,** 109-124.

934 Nielsen S.G., Rehkämper M., Porcelli D., Andersson P.S., Halliday A.N., Swarzenski P.W.,
935 Latkoczy C. and Günther D. (2005) The thallium isotope composition of the upper continental
936 crust and rivers - an investigation of the continental sources of dissolved marine thallium.
937 **Geochimica et Cosmichica Acta, 69,** 2007-2019.

938 Nielsen S.G., Rehkämper M. and Halliday A.N. (2006a) Large thallium isotopic variations in iron
939 meteorites and evidence for lead-205 in the early solar system. **Geochimica et Cosmochimica**
940 **Acta. 70,** 2643-2657.

941 Nielsen S.G., Rehkämper M., Norman M.D., Halliday A.N. and Harrison D. (2006b) Thallium
942 isotopic evidence for ferromanganese sediments in the mantle source of Hawaiian basalts. **Nature,**
943 **439,** 314-317.

944 Nielsen S.G., Rehkämper M., Teagle D.A.H., Alt J.C., Butterfield D. and Halliday A.N. (2006c)
945 Hydrothermal fluid fluxes calculated from the isotopic mass balance of thallium in the ocean crust.
946 **Earth and Planetary Science Letters, 251,** 120-133

947 Nielsen S.G., Rehkämper M., Brandon A.D., Norman M.D., Turner S. and O'Reilly S. Y. (2007)
948 Thallium isotopes in Iceland and Azores lavas – implications for the role of altered crust and
949 mantle geochemistry. **Earth and Planetary Science Letters, 264,** 332-345.

950 Nielsen S.G., Goff M., Hesselbo S.P., Jenkyns H.C., LaRowe D.E. and Lee, C.-T.A. (2011)
951 Thallium isotopes in early diagenetic pyrite – a palaeoredox proxy? **Geochimica et**
952 **Cosmochimica Acta, 75,** 6690-6704.

953 Nielsen S.G., Wasylenki L.E., Rehkämper M., Peacock C.L., Xue Z. and Moon E.M. (2013)
954 Towards an understanding of thallium isotope fractionation during adsorption to manganese
955 oxides. **Geochimica et Cosmochimica Acta, 117,** 252-265.

956 Nielsen S.G., Shimizu N., Lee C.T.A. and Behn M. (2014) Chalcophile behavior of thallium during
957 MORB melting and implications for the sulfur content of the mantle. **Geochemistry Geophysics**
958 **Geosystems, 15,** 4905-4919.

959 Nielsen S.G., Klein F., Kading T., Blusztajn J. and Wickham K. (2015) Thallium as a tracer of
960 fluid-rock interaction in the shallow Mariana forearc. **Earth and Planetary Science Letters, 430,**
961 416-426.

962 Nielsen S.G., Yogodzinski G.M., Prytulak J., Plank T., Kay S.M., Kay R.W., Blusztajn J., Owens
963 J.D., Auro M. and Kading T. (2016) Tracking along-arc sediment inputs to the Aleutian arc using
964 thallium isotopes. **Geochimica et Cosmochimica Acta, 181,** 217-237.

965 Nielsen S.G., Rehkämper M. and Prytulak J. (2017) Investigation and application of thallium
966 isotope fractionation. **In: Teng F.-Z., Watkins J. and Dauphas N. (eds), Reviews in Mineralogy**
967 **and Geochemistry 82: Non-traditional stable isotopes. Mineralogical Society of America**
968 **(USA)**, 759-798.

969 Nriagu J. (1998) Thallium in the Environment. **Wiley (New York),** 304pp.

970 Ostic R.G., El-Badry H.M. and Kohman T.P. (1969) Isotopic composition of meteoric thallium.
971 **Earth and Planetary Science Letters, 7,** 72-76.

972 Owens J.D., Nielsen S.G., Horner, T.J., Ostrander, C.M. and Peterson L.C. (2017) Thallium-

isotopic compositions of euxinic sediments as a proxy for global manganese-oxide burial. **Geochimica et Cosmochimica Acta, 213**, 291-307.

Palk C.S., Rehkämper M., Andreasen R. and Stunt A. (2011) Extreme cadmium and thallium isotope fractionations in enstatite chondrites. **Meteoritics and Planetary Science, 46,** A183-A183.

Park J.-W., Hu Z., Gao S., Campbell I.H. and Gong H. (2012) Platinum group element abundances in the upper continental crust revisited - new constraints from analyses of Chinese loess. **Geochimica et Cosmochimica Acta, 93,** 63-76.

Parks J., Lin S., Davis D.W., Yang X.-M., Creaser R.A. and Corkery M.T. (2014) Meso- and Neoarchean evolution of the Island Lake greenstone belt and the northwestern Superior Province: evidence from lithogeochemistry, Nd isotope data, and U–Pb zircon geochronology. **Precambrian Research, 246,** 160-179.

Peacock C.L. and Moon E.M. (2012) Oxidative scavenging of thallium by birnessite: explanation for thallium enrichment and stable isotope fractionation in marine ferromanganese precipitates. **Geochimica et Cosmochimica Acta, 84,** 297-313.

Peter A.L.J. and Viraraghavan T. (2005) Thallium: a review of public health and environmental concerns. **Environment International, 31,** 493-501.

Prytulak J., Nielsen S.G., Plank T., Barker M. and Elliott T. (2013) Assessing the utility of thallium and thallium isotopes for tracing subduction zone inputs to the Mariana arc. **Chemical Geology, 345,** 129-149.

Prytulak J., Brett E.K.A., Webb M., Rehkämper M., Plank T., Savage P.S. and Woodhead J. (2017) Thallium elemental behavior and stable isotope fractionation during magmatic processes. **Chemical Geology, 448,** 71-83.

Rehkämper M. and Halliday A.N. (1999) The precise measurement of Tl isotopic compositions by MC-ICPMS: application to the analysis of geological materials and meteorites. **Geochimica et Cosmochimica Acta, 63,** 935-944.

Rehkämper M. and Mezger K. (2000) Investigation of matrix effects for Pb isotope ratio measurements by multiple collector ICP-MS: verification and application of optimized analytical protocols. **Journal of Analytical Atomic Spectrometry, 15,** 1451-1460.

Rehkämper M., Frank M., Hein J.R., Porcelli D., Halliday A., Ingri J. and Liebetrau V. (2002) Thallium isotope variations in seawater and hydrogenetic, diagenetic, and hydrothermal ferromanganese deposits. **Earth and Planetary Science Letters, 197,** 65-81.

Rehkämper M. and Nielsen S.G. (2004) The mass balance of dissolved thallium in the oceans. **Marine Chemistry, 85,** 125-139.

Robin-Popieul C.C.M., Arndt N.T., Chauvel C., Byerly G.R., Sobolev A.V. and Wilson A. (2012) A new model for Barberton Komatiites: Deep critical melting with high melt retention. **Journal of Petrology, 53,** 2191-2229.

Schauble E.A. (2007) Role of nuclear volume in driving equilibrium stable isotope fractionation of mercury, thallium, and other very heavy elements. **Geochimica et Cosmochimica Acta, 71,** 2170-2189.

Shannon R.D. (1976) Revised effective ionic radii and systematic studies of interatomic distances in halides and chalcogenides. **Acta Crystallographica, A32,** 751-767.

Shannon R.D. and Prewitt C.T. (1969) Effective ionic radii in oxides and fluorides. **Acta Crystallographica, B25,** 925-946.

Shaw D.M. (1952) The geochemistry of thallium. **Geochimica et Cosmochimica Acta, 2,** 118-154.

Shu Y, Nielsen S.G., Zeng Z., Shinjo R., Blusztjan J., Wang X. and Chen S. (2017) Tracing subducted sediment inputs to the Ryukyu arc-Okinawa Trough system: Evidence from thallium isotopes. **Geochimica et Cosmochimica Acta, 217,** 462-491.

Smith C.N., Kesler S.E., Klaue B. and Blum J.D. (2005) Mercury isotope fractionation in fossil hydrothermal systems. **Geology, 33,** 825-828.

Snavely P.D. Jr., MacLeod N.S., Flanagan F.J., Berman S., Neiman H.G. and Bastron H. (1976) Nepheline syenite, STM-1, from Table Mountain, Oregon. **In: Flanagan F.J. (ed), Descriptions**

**and analyses of eight new USGS rock standards, United States, Geological Survey, Professional Paper, 840,** 7-10.

Søager N., Portnyagin M., Hoernle K., Holm P.M., Hauff F. and Garbe-Schönberg. (2015) Olivine major and trace element compositions in Southern Payenia Basalts, Argentina: evidence for pyroxenite-peridotite melt mixing in a back-arc setting. **Journal of Petrology, 56,** 1495-1518.

Stirling C.H., Andersen M.B., Potter E.-K. and Halliday A.N. (2007) Low-temperature isotopic fractionation of uranium. **Earth and Planetary Science Letters, 264,** 208-225.

Straub S.M. (2003) The evolution of the Izu Bonin - Mariana volcanic arcs (NW Pacific) in terms of major element chemistry. **Geophysics Geochemistry Geosystems, 4,** 1018, 33pp. 10.1029/2002GC000357.

Stromstoe N., Callow J.N., McGowan H.A. and Marx S.K. (2013) Attribution of sources to metal accumulation in an alpine tarn, the Snowy Mountains, Australia. **Environmental Pollution, 181,** 133-143.

Teng F.-Z., Watkins J. and Dauphas N. (eds). (2017) Reviews in Mineralogy and Geochemistry 82: Non-traditional stable isotopes. **Mineralogical Society of America (USA),** 732pp.

Timm C., Hoernle K.A., van den Bogaard P., Bindeman I.N. and Weaver S.D. (2009) Geochemical evolution of intraplate volcanism at Banks Peninsula, New Zealand: interaction between asthenospheric and lithospheric melts **Journal of Petrology, 50,** 989-123.

Turner S., Hoernle K., Hauff F., Johansen T.S., Klügel A., Kokfelt T. and Lundstrom C. (2015) $^{238}U$–$^{230}Th$–$^{226}Ra$ disequilibria constraints on the magmatic evolution of the Cumbre Vieja volcanics on La Palma, Canary Islands. **Journal of Petrology, 56,** 1999-2024.

Urey H.C. (1947) The thermodynamic properties of isotopic substances. **Journal of the Chemical Society (Resumed),** 562-581.

Uysal I.T., Gasparon M., Bolhar R., Zhao J.-x., Feng Y.-x. and Jones G. (2011) Trace element composition of near-surface silica deposits - a powerful tool for detecting hydrothermal mineral

and energy resources. **Chemical Geology, 280,** 154-169.

van der Straaten F., Schenk V., John T. and Gao J. (2008) Blueschist-facies rehydration of eclogites (Tian Shan, NW-China): implications for fluid–rock interaction in the subduction channel. **Chemical Geology, 255,** 195-219.

Vaněk A., Grösslová Z., Mihaljevič M., Ettler V., Trubač J., Chrastný V., Penížek V., Teper L., Cabala J., Voegelin A. and Zádorová T. (2018) Thallium isotopes in metallurgical wastes/contaminated soils: a novel tool to trace metal source and behaviour. **Journal of Hazardous Materials, 343,** 78-85.

Vink B.W. (1993) The behaviour of thallium in the (sub) surface environment in terms of Eh and pH. **Chemical Geology, 109,** 119–123.

Wang Z., Becker H. and Wombacher F. (2015) Mass fractions of S, Cu, Se, Mo, Ag, Cd, In, Te, Ba, Sm, W, Tl and Bi in geological reference materials and selected carbonaceous chondrites determined by isotope dilution ICP-MS. **Geostandards and Geoanalytical Research, 39,** 185-208.

Wehrmann H., Hoernle K., Garbe-Schönberg D., Jacques G., Mahlke J. and Schumann K. (2014) Insights from trace element geochemistry as to the roles of subduction zone geometry and subduction input on the chemistry of arc magmas. **International Journal of Earth Sciences, 103,** 1929-1944.

Weis D., Kieffer B., Maerschalk C., Barling J., de Jong J., Williams G.A., Hanano D., Pretorious W., Mattielli N., Scoates J.S., Goolaerts A., Friedman R.M. and Mahoney J.B. (2006) High-precision isotopic characterization of USGS reference materials by TIMS and MC-ICP-MS. **Geochemistry Geophysics Geosystems, 7,** Q08006, 30pp. 10.1029/2006GC001283.

White W.M., Albarède F. and Télouk P. (2000) High-precision analysis of Pb isotope ratios by multi-collector ICP-MS. **Chemical Geology, 167,** 257-270.

Wilson S.A. (1997a) The collection, preparation, and testing of USGS reference material BCR-2, Columbia River, basalt. **USGS Open-File Report** (in progress).

1076 Wilson S.A. (1997b) Data compilation for reference material BHVO-2, Hawaiian Basalt. **USGS**
1077 **Open-File Report** (in progress).

1078 Wilson S.A. (1998) Data compilation for reference material GSP-2, Granodiorite, Silver Plume,
1079 Colorado. **USGS Open-File Report** (in progress).

1080 Woodhead J., Hergt J., Greig A. and Edwards L. (2011) Subduction zone Hf-anomalies: mantle
1081 messenger, melting artefact or crustal process? **Earth and Planetary Science Letters, 304,** 231-
1082 239.

1083 Worthington T.J., Hekinian R., Stoffers P., Kuhn T. and Hauff F. (2006) Osbourn Trough:
1084 Structure, geochemistry and implications of a mid-Cretaceous paleospreading ridge in the South
1085 Pacific. **Earth and Planetary Science Letters, 245,** 685-701.

1086 Xiao T.F., Boyle D., Guha J., Rouleau A., Hong Y.T. and Zheng B.S. (2003) Groundwater-related
1087 thallium transfer processes and their impacts on the ecosystem: southwest Guizhou Province, China.
1088 **Applied Geochemistry, 18,** 675-691.

1089 Xiao T.F., Guha J., Boyle D., Liu C.Q. and Chen J.G. (2004) Environmental concerns related to
1090 high thallium levels in soils and thallium uptake by plants in southwest Guizhou, China. **Science**
1091 **of the Total Environment, 318,** 223-244.

1092 Xie Q., Liu S., Evans D., Dillon P. and Hintelmann H. (2005) High precision Hg isotope analysis of
1093 environmental samples using gold trap-MC-ICP-MS. **Journal of Analytical Atomic**
1094 **Spectrometry, 20,** 515–522.

1095 Yang S. and Liu Y. (2015) Nuclear volume effects in equilibrium stable isotope fractionations of
1096 mercury, thallium and lead. **Scientific Reports, 5,** 5:12626, 12pp. 10.1038/srep12626.

1097 Yokoyama T., Makishima A. and Nakamura E. (1999) Evaluation of the coprecipitation of
1098 incompatible trace elements with fluoride during silicate rock dissolution by acid digestion.
1099 **Chemical Geology, 157,** 175-187.

1100 Yu Z., Robinson P., Townsend A.T., Münker C. and Crawford A.J. (2000) Determination of high
1101 field strength elements, Rb, Sr, Mo, Sb, Cs, Tl and Bi at ng $g^{-1}$ levels in geological reference

materials by magnetic sector ICP-MS after HF/$HClO_4$ high pressure digestion. **Geostandards Newsletter, 24,** 39-50.

Yu Z., Robinson P. and McGoldrick P. (2001) An evaluation of methods for the chemical decomposition of geological materials for trace element determinations using ICP-MS. **Geostandards Newsletter, 25,** 199-217.

Zhang W., Hu Z., Liu Y., Chen L., Chen H., Li M., Zhao L., Hu S. and Gao S. (2012) Reassessment of HF/$HNO_3$ decomposition capability in the high-pressure digestion of felsic rocks for multi-element determination by ICP-MS. **Geostandards and Geoanalytical Research, 36,** 271-289.

# FIGURES

**Figure 1.** Comparison of Tl mass fractions obtained when using geological versus synthetic calibrators (see text for details). Both sets of measurements were performed using the same ICP-QQQ-MS instrument (Open University) and on the same solutions. Error bars are smaller than symbols in most cases.

**Figure 2.** Comparison of Tl mass fractions obtained during MC-ICP-MS isotope analysis and those determined by ICP-QQQ-MS (using geological reference materials as calibrators). Some error bars are smaller than symbols.

**Figure 3.** Tl isotope ratios (as $\varepsilon^{205}Tl_{SRM997}$; error bars: 2s) and Tl mass fractions (error bars indicate a conservative RSD of 20%) of RMs determined by MC-ICP-MS for (a) whole rock and (b) partially separated mineral reference materials. Shown are data for each individual digestion and the mean values for each RM. Thallium mass fraction data obtained via MC-ICP-MS simultaneously with isotope ratio measurement is used to aid qualitative assessment of material heterogeneity.

**Figure 4.** Tl isotope ratios (as $\varepsilon^{205}Tl_{SRM997}$) determined for the Aldrich Tl solution, relative to NIST SRM 997, over the course of 18 analytical sessions. The number of measurements made during each session is shown in brackets, and the error bars indicate the precision (2*s*) calculated from those measurements for each analytical session. The overall long-term intermediate precision of session averages (2*s*) is displayed as a grey band.

**Figure 5.** Variation of Tl mass fraction with $K_2O$ mass fraction for all materials except sulphide 14P. Error bars are smaller than symbols. All $K_2O$ data is as listed by the material's supplier. Tl mass fractions were determined by ICP-QQQ-MS at the Open University.

**Figure 6.** Assessment of relationship between test portion size of dissolved sample and isotope ratio variance (2*s*). For the digested sample mass, the plotted point represents the mean mass weighted by the number of measurements made per dissolution; error bars represent the full range of masses digested for each sample. Points are coloured according to Tl mass fraction as determined by ICP-QQQ-MS.

**Table 1: Literature MC-ICP-MS Tl isotope ratio data for igneous reference materials**

| Reference Material | $\varepsilon^{205}$Tl | 2*s* | # dissolutions | # measurements | Reference |
|---|---|---|---|---|---|
| AGV-2 | -1.9 | 0.5 | 1 | 1 | Baker *et al.* (2009) |
| AGV-2 | -3 | 0.6 | 8 | 15 | Prytulak *et al.* (2013) |
| AGV-2 | -2.7 | 0.2 | 5 | 9 | Prytulak *et al.* (2017) |
| BCR-2 | -2.5 | 0.4 | 4 | 19 | Prytulak *et al.* (2013) |
| BCR-2 | -2.5 | 0.5 | 12 | 25 | Prytulak *et al.* (2017) |
| BIR-1 | 1.1 | 1.2 | 6 | 9 | Nielsen *et al.* (2007) |
| BHVO-1 | -3.5 | 0.5 | 10 | | Nielsen *et al.* (2015) |
| BHVO-1 | -3.6 | 0.4 | | 16 | Shu *et al.* (2017) |
| BHVO-2 | -2.1 | 0.5 | 2 | 2 | Baker *et al.* (2009) |
| BHVO-2 | -1.5 | 0.4 | 2 | 2 | Prytulak *et al.* (2013) |
| BHVO-2 | -1.5 | 0.3 | 10 | n.g. | Coggon *et al.* (2014) |
| G-2 | 1.3 | 0.7 | 1 | 1 | Rehkämper and Halliday (1999) |

# dissolutions: number of independent digestions

# measurements: number of measurement results

## Table 2: Reference materials investigated in this study

| Reference Material | Supplier[a] | Lithology | Key reference | reported Tl mass fraction | reported $\varepsilon^{205}$Tl |
|---|---|---|---|---|---|
| 14P | OREAS | massive magmatic sulphide | - | | |
| AL-I | SARM-CRPG/CNRS | albite | Govindaraju (1984a) | | |
| AN-G | SARM-CRPG/CNRS | anorthosite | Govindaraju (1980) | | |
| BCR-2 | USGS | basalt | Wilson (1997a) | x | x |
| BHVO-2 | USGS | basalt | Wilson (1997b) | x | x |
| COQ-1 | USGS | carbonatite | - | | |
| FK-N | SARM-CRPG/CNRS | alkali feldspar | Govindaraju (1984b) | | |
| G-2[b] | USGS | granite | Fairbairn *et al.* (1951) | x | x |
| GSP-2 | USGS | granodiorite | Wilson (1998) | x | |
| ISH-G | SARM-CRPG/CNRS | trachyte | Gillot *et al.* (1992) | x | |
| MDO-G | SARM-CRPG/CNRS | trachyte | Gillot *et al.* (1992) | | |
| Mica-Fe | SARM-CRPG/CNRS | biotite | Govindaraju (1979) | x | |
| Mica-Mg | SARM-CRPG/CNRS | phlogopite | Govindaraju (1979) | | |
| SRM 607 | NIST | alkali feldspar | Heinrich (1960) | | |
| STM-1[b] | USGS | nepheline syenite | Snavely *et al.* (1976) | x | |
| UB-N | SARM-CRPG/CNRS | serpentinite | Govindaraju (1982) | | |

[a] OREAS: Ore Research & Exploration Assay Standards (Australia); SARM-CRPG/CNRS: Service d'Analyse des Roches et des Minéraux - Centre de Recherches Pétrographiques et Géochimiques/Centre National de la Recherche Scientifique (France); USGS: United States Geological Survey.

[b] No longer available for purchase.

**Table 3: Anion exchange separation of Tl (adapted from Nielsen *et al.* 2004)**

| | | Volume (ml) | |
|---|---|---|---|
| **Step** | **Eluent** | **Stage I** | **Stage II** |
| load resin | AG® 1-X8 (200–400 mesh) in 0.1 mol $l^{-1}$ HCl | 1 | 0.15 |
| condition | 0.1 mol $l^{-1}$ HCl – 5% w/w $SO_2$ | 1 + 10 | 0.1 + 1.5 |
| condition | 0.1 mol $l^{-1}$ HCl | 1 + 10 | 0.1 + 1.5 |
| condition | 1 mol $l^{-1}$ HCl – 1 % v/v $Br_2$ | 1 + 3 + 1 | 0.1 + 0.3 + 0.3 + 0.3 |
| load sample | 1 mol $l^{-1}$ HCl – 3 % v/v $Br_2$ | - | - |
| elution (matrix) | 0.5 mol $l^{-1}$ $HNO_3$– 3% v/v $Br_2$ | 1 + 1 + 1 + 5 + 10 | 0.1 + 0.1 + 0.1 + 1.5 |
| elution (matrix) | 2 mol $l^{-1}$ $HNO_3$– 3% v/v $Br_2$ | 1 + 1 + 4 + 10 | 0.1 + 1.5 |
| elution (matrix) | 0.1 mol $l^{-1}$ HCl – 1% v/v $Br_2$ | 1 + 1 + 4 + 10 | 0.1 + 1.5 |
| Tl elution | 0.1 mol $l^{-1}$ HCl – 5% w/w $SO_2$ | 1 + 1 + 1 + 3 + 9 + 1 | 0.1 + 1.5 |

**Table 4: Thallium mass fraction data obtained during this study, and comparison with literature data**

| Reference Material | # dissolutions | # measurements (n) | [Tl] (ng $g^{-1}$) | RSD % | References |
|---|---|---|---|---|---|
| ***Calibrators*** | | | | | |
| **AGV-1** | | | *349* | *14.9* | *7,8,13,17,24,25,33,34,49,50,53,55* |
| | | | *337* | *4.7* | *28 (GeoReM preferred value)* |
| **BHVO-2** | 2 | 6 | 23 | 4.9 | This study* |
| | | | *22* | *20* | *1,2,5,6,8-10,16,20,21,23,25-27,30,31,36-41, 43,45,48,49,51-53,58* |
| | | | *22.4* | *20* | *28 (GeoReM preferred value)* |
| **BIR-1** | 3 | 15 | 1 | 21 | This study* |
| | | | *1.8* | *41* | *1,8,18,25,32,35,42,46,47,53-56* |
| | | | *2.1* | *34* | *28 (GeoReM preferred value)* |
| ***Measured reference materials*** | | | | | |
| **14P** | 3 | 10 | 100† | 20 | This study |
| **AL-I** | 1 | 2 | 42 | 8.3 | This study |
| **AN-G** | 1 | 1 | 10 | 8.0 | This study |
| **BCR-2** | 3 | 19 | 306 | 6.7 | This study |
| | | | *265* | *13* | *3,10,12,14,15,19-22,25,26,29,36-38,40,41, 43,45,58* |
| | | | *267* | *13* | *28 (GeoReM preferred value)* |
| **COQ-1** | 1 | 7 | 96 | 3.9 | This study |
| **FK-N** | 1 | 1 | 3720 | 0.5 | This study |

| | | | | | |
|---|---|---|---|---|---|
| **G-2** | 1 | 1 | 940 | 6.6 | This study |
| | | | *888* | *3.1* | *18,23,25,26,28,50,57,58* |
| | | | *884* | *3.0* | *28 (GeoReM preferred value)* |
| **GSP-2** | 2 | 4 | 1500 | 5.4 | This study |
| | | | *1290* | *7.9* | *26,36,58* |
| **ISH-G** | 1 | 1 | 790 | 0.7 | This study |
| **MDO-G** | 1 | 1 | 61 | 2.0 | This study |
| **Mica-Fe** | 1 | 1 | 16800 | 0.4 | This study |
| | | | *16000* | *n.g.* | *4,11,44* |
| **Mica-Mg** | 1 | 1 | 5270 | 0.8 | This study |
| **SRM 607** | 1 | 1 | 2650 | 1.1 | This study |
| **STM-1** | 1 | 1 | 260 | 1.4 | This study |
| | | | 220 | 6.4 | 17,44 |
| **UB-N** | 1 | 2 | 41 | 4.3 | This study |
| | | | *49* | *18.3* | *8,17,46,52,56* |

* These Tl mass fraction results were obtained for solutions of the calibrator reference materials that were run as unknowns.
† Mass fraction estimated using MC-ICP-MS.

# dissolutions: number of independent digestions
# measurements: number of measurement results

References: (1) Babechuk *et al.* (2010), (2) Babechuk and Kamber (2011), (3) Baker *et al.* (2010), (4) Baranov *et al.* (2002), (5) Barnes *et al.* (2013), (6) Brandl *et al.* (2012), (7) Bolge *et al.* (2006), (8) Chauvel *et al.* (2011), (9) Chauvel *et al.* (2012), (10) Condomines *et al.* (2015), (11) Dampare *et al.* (2008), (12) Deng *et al.* (2013), (13) Eggins *et al.* (1997), (14) Elmaleh *et al.* (2012), (15) Espanon *et al.* (2014), (16) Gale *et al.* (2011), (17) Garbe-Schönberg (1993), (18) Gaschnig *et al.* (2015), (19) Geldmacher *et al.* (2008), (20) Gibson *et al.* (2013), (21) Gómez-Tuena *et al.* (2011), (22) González-Álvarez and Kerrich (2011), (23) He *et al.* (2010), (24) Hettmann *et al.* (2014), (25) Hu and Gao (2008), (26) Hu *et al.* (2013), (27) Jacques *et al.* (2013), (28) Jochum *et al.* (2016), (29) Kamber *et al.* (2005), (30) Kawabata *et al.* (2011), (31) Kirchenbauer *et al.* (2012), (32) Kodolányi *et al.* (2012), (33) Makishima and Nakamura (2006), (34) Makishima *et al.* (2011), (35) Martin *et al.* (2015), (36) Marx and Kamber (2010), (37) Marx *et al.* (2010), (38) McCoy-West *et al.* (2010), (39) Mohan *et al.* (2013), (40) Mori *et al.* (2007), (41) Mori *et al.* (2009), (42) Nielsen *et al.* (2007), (43) Park *et al.* (2012), (44) Parks *et al.* (2014), (45) Prytulak *et al.* (2013), (46) Robin-Popieul *et al.* (2012), (47) Søager *et al.* (2015), (48) Stromsoe *et al.* (2013), (49) Timm *et al.* (2009), (50) Uysal *et al.* (2011), (51) van der Straaten *et al.* (2008), (52) Wang *et al.* (2015), (53) Wehrmann *et al.* (2014), (54) Woodhead *et al.* (2011), (55) Worthington *et al.* (2006), (56) Yu *et al.* (2000), (57) Yu *et al.* (2001), (58) Zhang *et al.* (2012).

**Table 5: Thallium isotope ratio measurement results obtained during this study**

| Reference Material | # dissolutions | # sessions | # measurements | $\varepsilon^{205}$Tl | 2*s* |
|---|---|---|---|---|---|
| **14P** | 3 | 1 | 10 | -2.0 | 0.5 |
| **AL-I** | 3 | 3 | 5 | -1.5 | 0.2 |
| **AN-G** | 3 | 3 | 3 | -2.7 | 0.4 |
| **BCR-2** | 3 | 1 | 5 | -2.4 | 0.2 |
| **BHVO-2** | 3 | 3 | 4 | -1.2 | 0.7 |
| **COQ-1** | 3 | 2 | 5 | -2.3 | 0.5 |
| **FK-N** | 3 | 4 | 11 | -0.1 | 0.7 |
| **G-2** | 3 (1) | 3 | 10 | -2.3 | 2.0 |
| **GSP-2** | 3 (1) | 2 | 9 | -2.5 | 0.6 |
| **ISH-G** | 3 (1) | 3 | 9 | -1.5 | 0.5 |
| **MDO-G** | 3 (1) | 3 | 7 | 0.5 | 0.7 |
| **Mica-Fe** | 3 | 4 | 11 | -3.4 | 0.7 |
| **Mica-Mg** | 3 | 4 | 12 | -0.1 | 0.9 |
| **SRM 607** | 3 | 2 | 9 | -3.1 | 0.8 |
| **STM-1** | 3 (1) | 2 | 10 | -2.0 | 1.1 |
| **UB-N** | 3 | 3 | 5 | 1.8 | 0.4 |

# dissolutions: total number of independent digestions; (X) gives the number of bomb digestions
# sessions: number of analytical sessions during which the RM was analysed
# measurements: number of separate analyses

# Figure 1

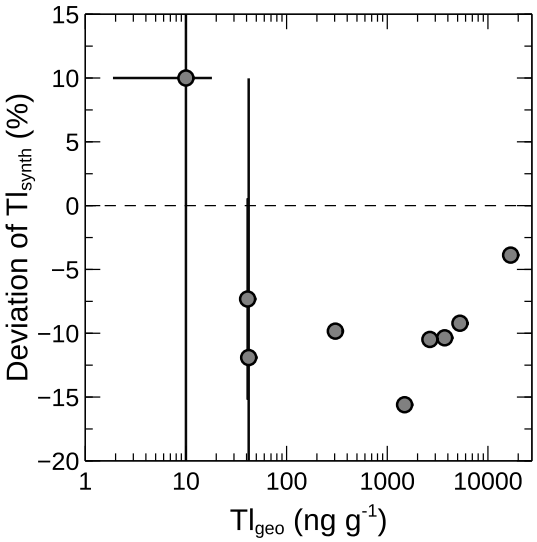
15
10
5
0
−5
−10
−15
−20
1
10
100
1000
10000
Deviation of Tl$_{synth}$ (%)
Tl$_{geo}$ (ng g$^{-1}$)

# Figure 2

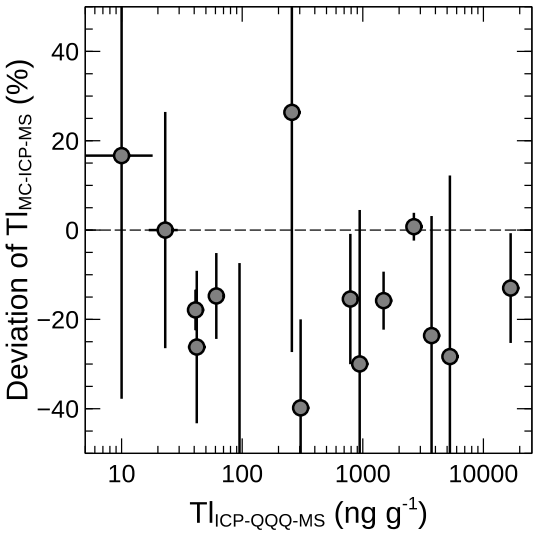
40
20
0
−20
−40
10
100
1000
10000
Deviation of $Tl_{MC\text{-}ICP\text{-}MS}$ (%)
$Tl_{ICP\text{-}QQQ\text{-}MS}$ (ng $g^{-1}$)

# Figure 3a

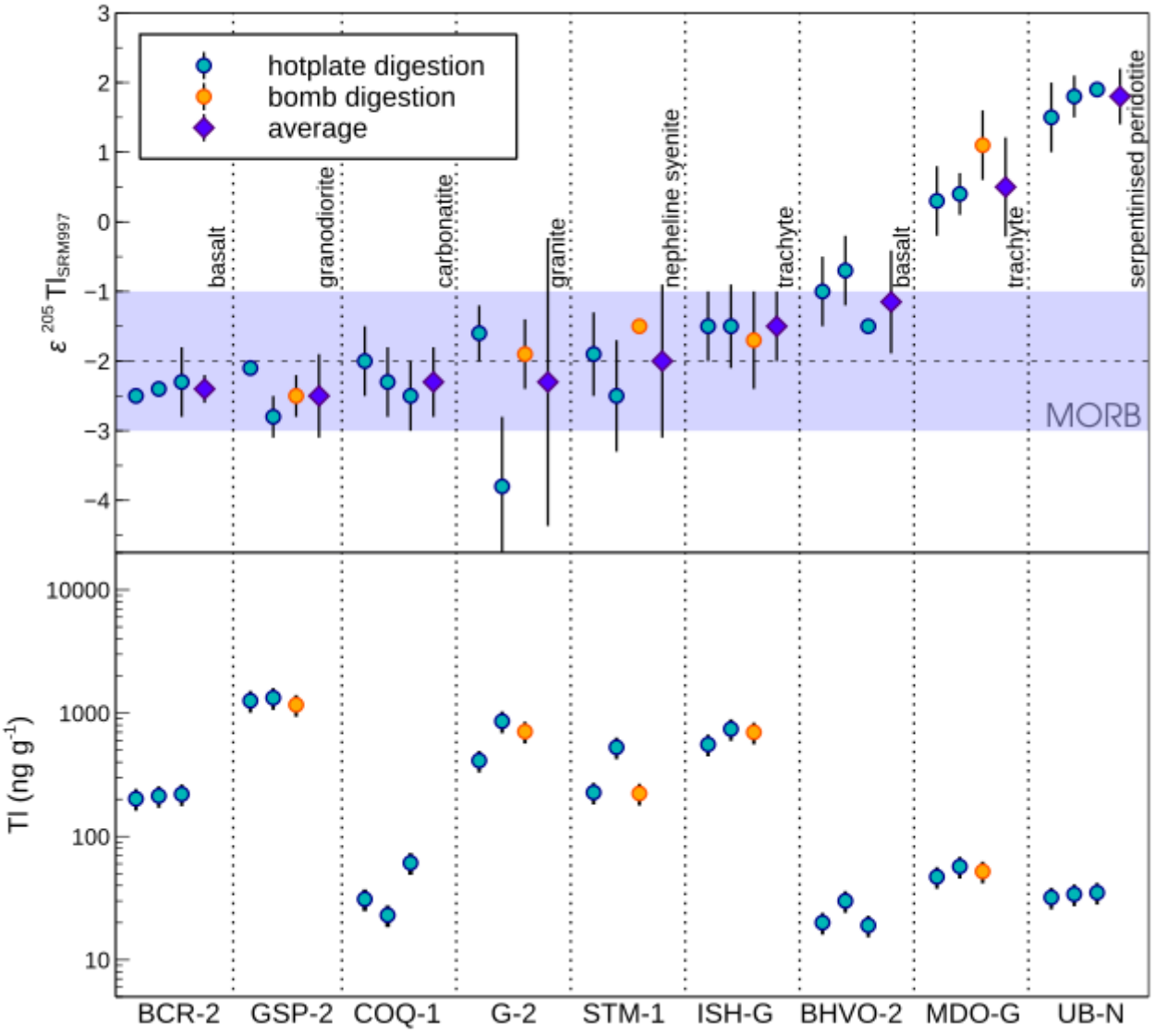
hotplate digestion
bomb digestion
average
basalt
granodiorite
carbonatite
granite
nepheline syenite
trachyte
basalt
trachyte
serpentinised peridotite
MORB
ε 205 Tl SRM997
Tl (ng g-1)
BCR-2
GSP-2
COQ-1
G-2
STM-1
ISH-G
BHVO-2
MDO-G
UB-N

# Figure 3b

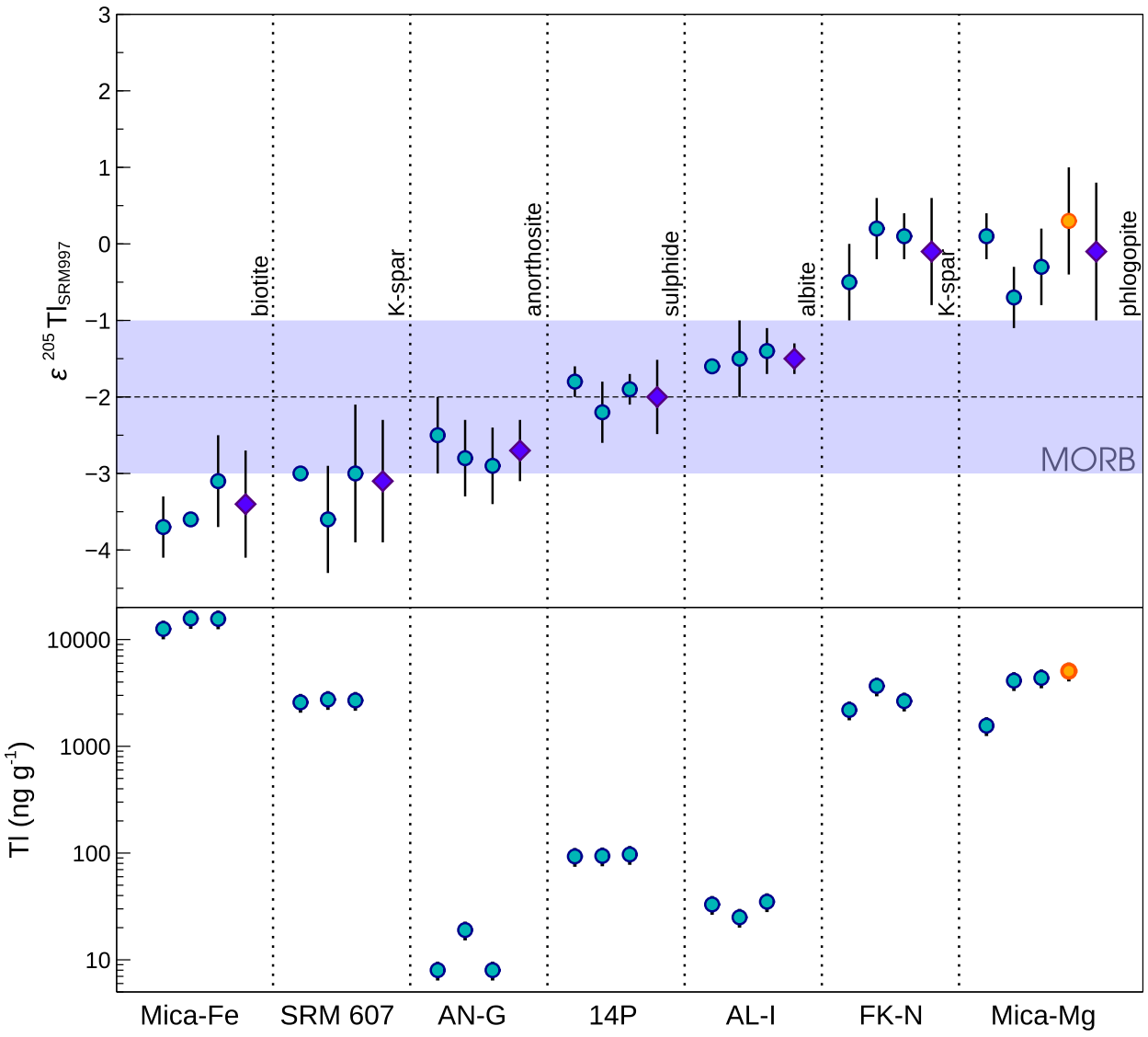
3
2
1
0
−1
−2
−3
−4
ε 205 TlSRM997
biotite
K-spar
anorthosite
sulphide
albite
K-spar
phlogopite
MORB
10000
1000
100
10
Tl (ng g-1)
Mica-Fe
SRM 607
AN-G
14P
AL-I
FK-N
Mica-Mg

# Figure 4

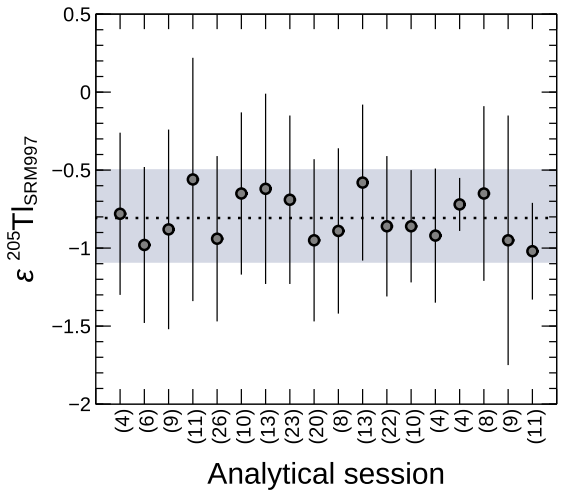
0.5
0
−0.5
−1
−1.5
−2
ε 205Tl SRM997
(4)
(6)
(9)
(11)
(26)
(10)
(13)
(23)
(20)
(8)
(13)
(22)
(10)
(4)
(4)
(8)
(9)
(11)
Analytical session

# Figure 5

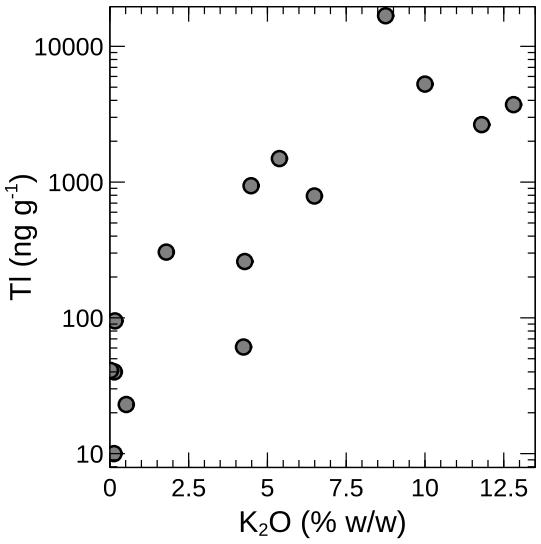

# Figure 6

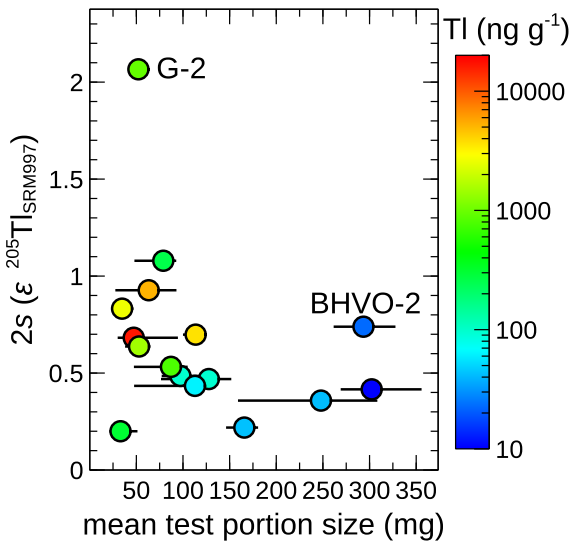
Tl (ng g-1)
10000
1000
100
10
G-2
BHVO-2
2s (ε 205Tl/SRM997)
0
0.5
1
1.5
2
50 100 150 200 250 300 350
mean test portion size (mg)